1-1-2013

High Performance RF Control Devices Using Capacitively Coupled Contacts (C3) Over III-N Heterostructures

Faisal Jahan
University of South Carolina

HIGH PERFORMANCE RF CONTROL DEVICES USING CAPACITIVELY COUPLED CONTANCTS (C3) OVER III-N HETEROSTRUCTURES

by

Faisal Jahan

Bachelor of Science
University of Dhaka, 2009

Master of Engineering
University of South Carolina, 2011

Submitted in Partial Fulfillment of the Requirements

For the Degree of Doctor of Philosophy in

Electrical Engineering

College of Engineering and Computing

University of South Carolina

2013

Accepted by:

Grigory Simin, Major Professor

Mohammod Ali, Committee Member

Guoan Wang, Committee Member

Jamil Khan, Committee Member

Lacy Ford, Vice Provost and Dean of Graduate Studies

DEDICATION

Dedicated to the three most important women in my life; my mother, sister and wife- without their support and sacrifices this work would never be possible.

ACKNOWLEDGEMENTS

First and foremost, I would like to thank my advisor Professor Grigory Simin for his continuous guidance, support and encouragement throughout my research. I started with zero knowledge of the world four years ago, as well as of myself, and under his guidance came out today to be a self-motivated individual , carrying not only a small portion of his vast knowledge and experiences, but also his optimism and methodology in getting through obstacles, both in research and in life. I am ever grateful to him for his endless care in this four years, I always felt lucky to have him as my advisor. His supervision always proved to be fruitful in my research work. I do not have words to thank him for all his support, help and guidance during my time in University of South Carolina.

I am grateful to my PhD dissertation committee members, Professor Mohammod Ali, Dr. Guoan Wang and Professor Jamil Khan for their invaluable suggestions and constant inspiration.

I would like to thank all my current and past colleagues in the Microwave Microelectronics research group. I would specially like to thank my past colleagues Jingbo and Bilal for helping me getting trained with all the characterization tools and also for their support, suggestions and valuable discussions in research. I would also thank my current colleague Yi-Hsuan for her continuous support on simulation which has greatly helped to achieve my research goals.

I am thankful to all the people from Sensor Electronic Technology Inc. for their flawless works on fabrication of III-Nitride Heterostructure Varactors. Their continuous improvement in device technology in terms of superior wafer and device quality has given a great advantage for my design.

Finally, I would like to express my gratitude towards my friends and family members for their endless support.

ABSTRACT

RF switches, power limiters and other control devices are essential components of modern RF systems. RF switches are important parts of wireless modules of various devices such as laptops, tablets, cell phones etc. and key components of satellites communication systems, radars, multi-band wireless and aerospace communications, phased array antennas. RF Power limiters (PL) are also important components of RF systems protecting linear amplifiers, detectors etc. from high-power stress. Traditionally, RF switches are fabricated using pin diodes or MEMS, Si MOSFETs or GaAs HEMTs. RF PLs are typically implemented using Schottky or pin-diodes. Traditional devices used in RF switch and PLs have a number of disadvantages and limitations. Si or GaAs based devices suffer from a low breakdown voltage and cannot handle high RF power. Pin-diodes require large forward currents and do not allow for fast turn-on. III-Nitride heterostructures open tremendous opportunities for RF control devices due to the record high sheet electron density in the 2D channel, extremely low channel resistance, high breakdown field and excellent temperature stability. In this dissertation a novel type of RF component using two-terminal III-Nitride heterostructure varactor with capacitively-coupled contacts (C^3) is introduced which can be used as a RF switch as well as a power limiter or other control device type.This C^3 varactor consists of two electrodes deposited on top of an AlGaN/GaN heterostructure forming capacitors between the electrode and the 2DEG channel. C^3 electrodes allow for efficient RF signal injection into the 2DEG channel with low equivalent impedance at high frequencies. The C^3 varactor has simple

planar structure fully compatible with MMICs. The III-N C^3 varactors have significant advantages over III-N heterostructure field-effect transistors (HFETs) as they allow for shorter channel, do not have gates or ohmic contacts and hence the fabrication is alignment- and anneal - free, they do not consume DC current and provide the DC block. The fabricated SPST C^3 switch exhibits 0.8 dB loss and 27 dB isolation at 18 GHz. The maximum switching power extrapolated from 2 GHz data is around +38 dBm. The fabricated PLs show 0.2-0.7 dB loss and limiting powers range from 17 to 40 dBm. The switching response is also very fast as it is in the ns range. The C^3 PL shows superior performance compared to other known types, e.g. Schottky diode PLs. The fabricated C^3 PLs and switches showed the output power variations within 0.5 dB during 100 hours of CW stress. They also demonstrated as low as 0.5 dB loss increase degradation at 200^o C as compared to the room temperature performance. The achieved results show that novel C^3 RF components have superior performance characteristics, can operate in a broad frequency range, and have a great potential for high-performance MMICs.

TABLE OF CONTENTS

LIST OF FIGURES

List of Abbreviations

PL ..... Power Limiter

C3 ..... Capacitively Coupled Contacts

2DEG ..... Two Dimensional Electron Gas

MEMS ..... Micro Electro Mechanical Systems

IL ..... Insertion Loss

IS ..... Isolation

CHAPTER 1

INTRODUCTION TO RF CONTROL DEVICES

1.1 RF Switches and Applications

RF switches are passive components controlled electrically to pass, block, and/or redirect electrical signals oscillating at RF frequencies, which is defined from 300 MHz to 300 GHz, with most of the applications within 1 - 100 GHz range. The switch performances in ON/OFF state are evaluated by insertion loss and isolation. Apart from insertion loss and isolation other important figures of merit of RF switches are high power handling, fast switching speed, high temperature and harsh environment operation [1]. Insertion loss is the amount power lost in ON state while transmitting a signal from input port to output port. Isolation is a measure of how output port is isolated from input port in OFF state. In other words, how well the switch can transfer power, which is determined by the amount of power lost on the switch when the switch is passing RF signals through, called insertion loss. Insertion loss expressed in dB is the ratio of output power delivered to the load at the switch's output port and input power generated by the signal source, which is expressed as:

$$IL\ (dB) = Pout\ (dBm) - Pin\ (dBm)$$

When assuming matched condition, s-parameter between input and output port of the switch (S21) in ON-state is the switch's insertion loss; on the other hand how well the switch can block power, called isolation, which is measured in the same way as insertion

loss, but when the switch is in OFF-state. Another aspect is the maximum power the switch can transfer, which typically defined as the point of input power where insertion loss starts to drop by 0.1 dB or 1 dB, due to degradation of the switch at extremely high power, and is called 0.1 dB or 1 dB power compression point. There are many additional aspects that are less critical and fundamental than the previous three, but also important in practical application, such as return loss, noise, and linearity.

Ideally a single series element can act as control element. However the switch isolation degrades over the frequency range. One solution to address the problem is adding shunt element. In ON state series element is ON and shunt element is OFF and vice versa. Depending on the requirement a RF switch can be single pole single throw (SPST), single pole double throw (SPDT) to single pole n throws (SPnT) where n is an integer.

RF switching elements are key components of modern wireless communication systems. High/low power RF switching elements are important parts of wireless modules of various devices such as laptops, tablets, cell phones etc. (Figure 1.1). They are used in radar transceiver modules, multi-band wireless, aerospace communication systems and phase shifters for beam steering in phased array antenna technology [2], and other reconfigurable passive RF elements [3][4]. The development of phased array radar technology at Lincoln Laboratory dates back to 1958 [5].The state-of-art RF switches of such application are typically less than few mm^2 in device area, with less than 1 dB insertion-loss in ON-state and more than 25 dB isolation in OFF-state. Frequency range varies from several GHz to over 100 GHz, depending on application, while power

handling capability can be as low as in milliwatts or as high as tens of watts per each discrete device.Fig. 1.2 shows the block diagram of front end module of 3G base stations.

Figure 1.1 RF switch applications-Space Satellite, Satellite Car Radio, Pad

On the nature of native device RF switches can be broadly divided into two categories. One is Micro-electromechanical System (MEMS) Switches and the other one is Solid State Switches.

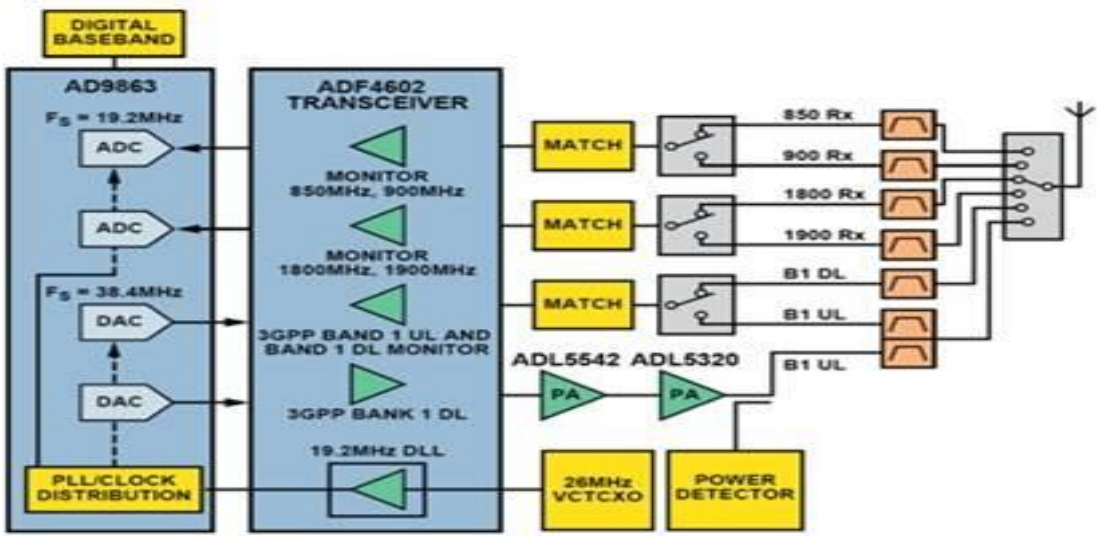

Figure 1.2 An example of the front-end module of 3G base-station

MEMS are micro-electromechancial system where physical movement of thin highly conducting membrane turns the switch in ON and OFF condition. In solid state switch the electronic flow/drought turns the switch in ON and OFF state respectively. Solid state switches are devices made of semiconductor materials and can be either bipolar or unipolar. In bipolar device (PIN diode) both electrons and holes participate in switch operation while in unipolar device either holes or electronic flow controls the switch. GaAs MESFETs (Metal Semiconductor Field Effect Transistor), AlGaAs/GaAs HEMTs (High Electron Mobility Transistor), III-Nitrides HFETs (Heterostructure Field Effect Transistor) and CMOS (Complementary Metal Oxide Semiconductor) Switches are examples of unipolar devices.

Radars, including multi-channel reconfigurable radars, satellite communication systems, Software Defined Radios (SDRs) and other systems require compact RF switches, power limiters, phase shifters and other control components with low loss, high switching power, high linearity, and low power consumption. None of existing RF devices fully and simultaneously meets these requirements.

Pin-diodes require at least 20 mA forward bias current to be turned on; they also need bias filters with bulky inductors and long switch settling time for high power operation[6][7].

The micro-electrical-mechanical system (MEMS) technology developed in the past decade has drawn much attention for its potential of delivering low loss and high isolation radio-frequency (RF)/microwave switching with compact size.[8][9] MEMS are vulnerable to hot switching, their switching times are limited to a few microseconds, and many MEMS subtypes require high operating voltage and vacuumed packaging.

Si MOSFETs and GaAs HEMTs suffer from low breakdown voltages and cannot achieve the required linearity levels due to nature of the material[10][11].

Gallium Nitride (GaN) MMICs are promising candidates to replace Silicon positive intrinsic negative (PIN) diodes and MEMS due to high frequency, low insertion loss, high isolation, high temperature, harsh environment operation, high ESD tolerance, reliability and fast switching speeds.

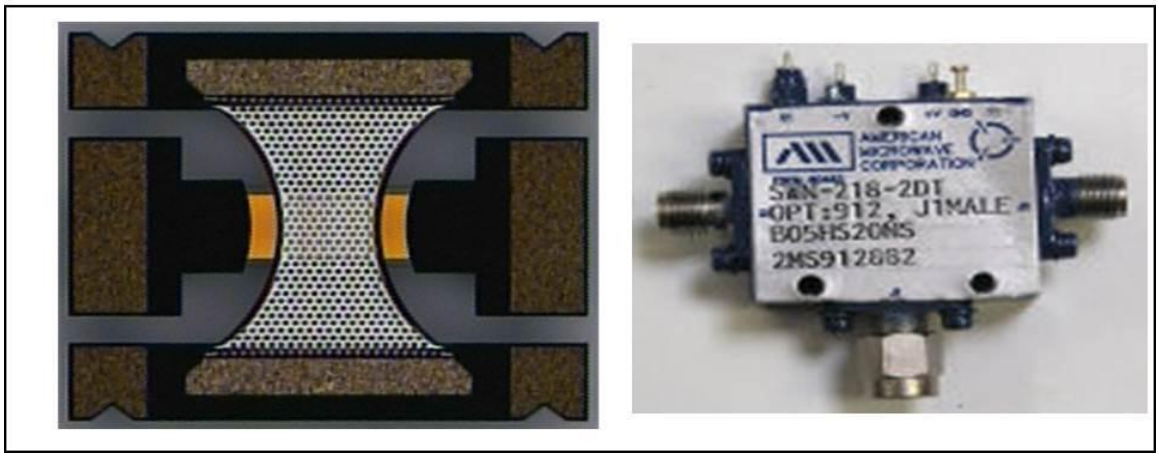

Figure 1.3 MEMS and PIN diode based RF switches

1.2 RF Power Limiters and Applications

RF Power limiters (PL), are also important components of RF systems protecting linear amplifiers, detectors etc. from high-power stress. In other words, the purpose of a limiter circuit is to protect power-sensitive microwave components by acting as a buffer against high-power signals [12]. A typical example is the radar T/R module where the high-power transmitter and low-noise amplifier are connected to the common antenna through a switch or circulator. As the power and component densities are going up in today's systems, the demand for fast, low-loss, high-temperature power limiters greatly increases.

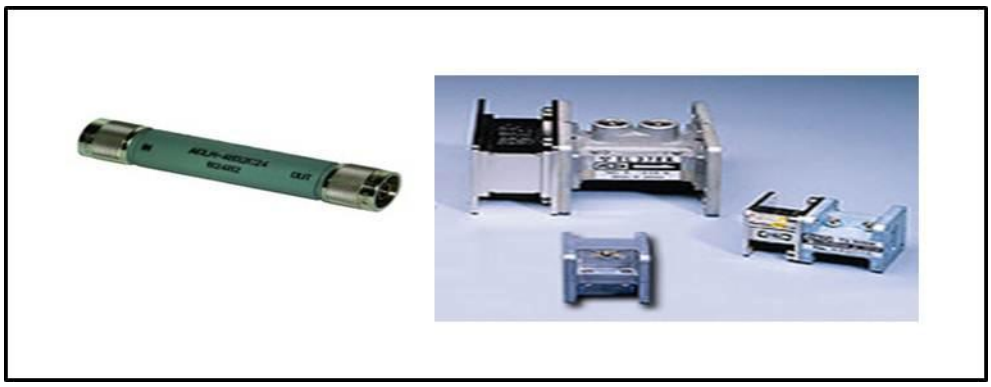

Figure 1.4 PIN diode based RF power limiter

Currently, the most widely used solid-state RF limiters are based on Schottky p-n or pin diodes and field-effect transistors, mainly based on Si, GaAs or SiC. Diode-type limiters are typically connected in shunt in the transmission line, where to achieve strong power limiting effects, large device area is required, which in turn leads to large capacitance and limited operating frequency range. This performance limitation applies to all types of diode limiters; Si, GaAs or SiC based. Junction diode limiters, especially

pin-diodes have relatively slow response time due to accumulation of minority carriers. GaAs limiters are typically of MESFET or HEMT types. Due to limited breakdown voltages and bandgap, high maximum powers and high operating temperatures cannot be obtained using GaAs or Si devices.

1.3 III-Nitride HFET as RF Switch

In 2002, R. Caverly and his colleague at Villanova University first explored possibility of using AlGaN/GaN heterjunction FET (HFET) as high power RF switch.[13] Soon afterwards, AlGaN/GaN HFET and later metal-oxide-semiconductor HFET (MOS-HFET) have demonstrated outstanding capability of high power, high frequency RF switching[14][15]. Although less matured as compared to power amplifiers, III-nitride RF switches have tremendous advantages over most other RF switch types, not only because of the material's high breakdown voltage and decent heat conductivity, but also the high density two-dimensional electron gas (2DEG) channel whose resistivity is comparable to that of metals [16]. Past efforts in III-Nitride materials and devices were mainly focused on power amplifiers; however many technology improvements resulting in lower channel and contact resistance, surface breakdown elimination etc. lead to high performance III-N switches with the best combination of low insertion loss, high isolation, high switching powers and speed among most of other switch types.

III-Nitride materials have numerous advantages over other materials. GaN a wide bandgap (3.4 eV) semiconductor, due to low intrinsic carrier concentrations allow better

device control at high temperatures. Another advantage of GaN over other wide bandgap semiconductors e.g. Silicon Carbide (SiC) is the heterojuction formation. As shown in Fig. 1.6, the electron mobility increases tremendously due to formation of two dimensional electronic gas (2DEG) at the interface of the heterojunction.

Compared with other material systems, III-N HFET has high saturation current, low channel resistance, high breakdown voltage, good thermal stability and thermal conductivity. Higher number of Johnson's figure of merit makes it ideal material for high power and high frequency applications. Since first demonstration of HFET in 1993 [17] GaN electronics both on active and passive devices has enjoyed great success due to focus of attention of various research groups. After 15 years of continuous attention by number of Scientists and Engineers around the globe, GaN technology is approaching to maturity and various commercial products have been announced in the recent years by number of semiconductor companies like TriQuint Semiconductor, Cree, Gain Microwave and RFMD etc.

	Si	GaAs	4H-SiC	GaN	Diamond
E_g (eV)	1.1	1.42	3.26	3.39	5.45
n_i (cm^{-3})	1.5×10^{10}	1.5×10^{6}	8.2×10^{-9}	1.9×10^{-10}	1.6×10^{-27}
ε_r	11.8	13.1	10	9.0	5.5
μ_n (cm^2/Vs)	1350	8500	700	1200(Bulk) 2000(2DEG)	1900
v_{sat} (10^7cm/s)	1.0	1.0	2.0	2.5	2.7
E_{br} (MV/cm)	0.3	0.4	3.0	3.3	5.6
Θ (W/cm K)	1.5	0.43	3.3-4.5	1.3	20
$JM = \frac{E_{br}v_{sat}}{2\pi}$	1	2.7	20	27.5	50

Figure 1.5 Electronic properties of semiconductor material systems [18]

Due to unavailability of native substrate GaN is grown over sapphire or SiC substrates. Heterojunction is formed at the interface of thin layer of AlGaN (15-20 nm) grown over thick layer (about 2 μm) of GaN crystal on top of a substrate. Unlike III-Arsenide, III-Nitride materials exhibit strong polarization. Polarization in AlGaN/GaN heterojunction can be divided into two types, i.e. spontaneous and piezoelectric polarization [16]. Spontaneous polarization is generally found in materials with wurtzite crystal structure. The electronegativity difference between Gallium (Ga) and nitrogen (N) atomic layer in GaN gives rise to spontaneous polarization pointing from Ga-face to N-face. Piezoelectric polarization only occurs in heterojunction due to difference in lattice constants between AlGaN and GaN layers. The thin AlGaN layer stretches over GaN and creates mechanical strain due to which atoms are forced to shift from their electrically neutral positions giving rise to piezoelectric polarization. By controlling growth conditions, layers thickness and aluminum (Al) concentration, both spontaneous and piezoelectric polarization can be oriented in the same direction enhancing the total effective polarization charge that attracts large number of free electrons at the heterojunction interface creating 2DEG in the channel. The concentration of electrons in this thin sheet forming the channel (2DEG) is ~ 2 x 10^{13} cm^{-2}. The 2DEG is electrically coupled with positive charges trapped at the top surface of AlGaN layer. The trapped surface charges are much less mobile than 2DEG, and therefore do not affect the operation of AlGaN/GaN as a transistor. Figure 1.6 shows a Heterostructure Field Effect Transistor (HFET). AlGaN/GaN HFET is a three terminal device similar to a regular field effect transistor (FET) in operation acting as a voltage controlled current source. Both source and drain forms ohmic contacts to 2DEG whereas gate metal forms schottky

contact. The bias voltage at the gate terminal modulates the current flow in the channel between source and drain contacts. AlGaN/GaN HFETs are normally ON devices forming a DC and/or RF path when a signal is applied at the input. Therefore with zero gate bias (V_G= 0V), these transistors are in ON state. When a negative gate voltage lower than device's threshold voltage ($V_G < V_{TH}$) is applied, the net negative charge on the gate electrode depletes the electrons in the channel under the gate as shown in the Fig 1.6 (d), the signal path is cut off and device is said to be in the OFF state behaving as a capacitor. In order to reduce the gate leakage current in conventional Schottky gate HFET various insulated gate technologies have been demonstrated such as metal oxide semiconductor (MOSHFET) [19][20], metal insulator semiconductor junctions (MISHFET) [21] etc. Typically value of threshold voltage is from -4 V for HFET and -8 V for MOSHFET.

When used as RF switches, the devices insertion loss is determined by the channel resistance and the two contact resistances whereas the isolation in OFF state is determined by the capacitance. Therefore in order to improve switch performance the product of both R_{ON}*C_{OFF} should be minimum. R_{ON} can be reduced by improving growth and device fabrication processes. C_{OFF} can be reduced by innovation in device layout. It has been shown that total C_{OFF} decreases with increase in number of gates. A thin metal gate is placed in the middle of the path. For power applications, the gate is placed closer to source than to drain, while for microwave switching, more than one gate can be used yet the geometry should be kept symmetrical. When negative bias is applied to the gate, its electric potential pushes away free electrons in the 2DEG channel beneath the gate. When the negative bias is high enough, channel beneath the gate can be completely

depleted, and the signal path from one ohmic to the other is then cut. Such voltage is called threshold voltage or pinch-off voltage, and is typically 4 - 6 V.

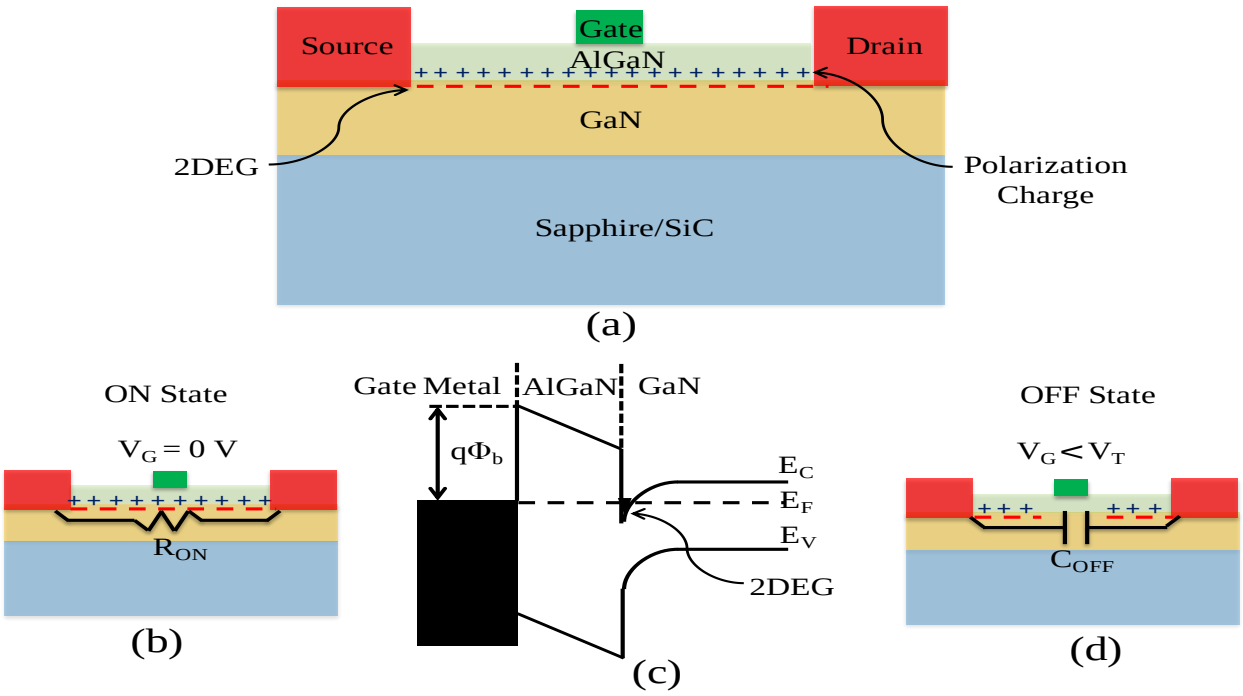

Figure 1.6 (a) Heterostructure Filed effect Transistor (HFET) (b) HFET in ON state (C) Band diagram showing Metal/AlGaN/GaN interface (d) HFET in OFF state

Multigate designs simultaneously increase the isolation and maximum switching powers [22]. Recently SPDT switches with hybrid fast/slow gate design also improved the switch transmission characteristics. Hybrid gate design reduces the C_{OFF} compared to conventional devices and has lower insertion loss and higher isolation [23].

1.4 Performance Limitations in III-N HFET RF Switch

Despite the outstanding performance of AlGaN/GaN HFET based switches, two major limitations, which are related both to the material properties and device design, hinder further improvement of such device.

First are the Ohmic contacts which are used as input and output electrodes.Unlike heavy doping in Si, ohmic contact on AlGaN is formed by quickly annealing a stack of specific metal layers at very high temperature, usually at 800 ^{o} to 900 ^{o} C for less than a minute[24]. The reason doping does not work on AlGaN is mostly due to the material's tough chemical nature and its very wide bandgap. The key player in rapid thermal annealing (RTA) process to form ohmic contact on AlGaN is the bottom Ti layer in the metal stack before annealing. Based on several studies on ohmic contact, at high temperatures Ti penetrates and reacts with AlGaN to form conducting TiN clusters and creates N vacancies inside AlGaN, which in addition act like n-type dopant to increase the affected region's conductivity. The penetration can be several tens of nanometers, enough to reach the heterojunction interface, where the 2DEG channel is. One theory suggests that it is the spikes of TiN penetrating through heterojunction that connect directly [25][26] to the 2DEG channel loosely preserved in the contact region (Figure 1.8).

Therefore the annealing condition should be carefully controlled in order to achieve optimum conductivity, for too low temperature or too short annealing time will not create enough penetration, while too high temperature or too long annealing time will flood the heterojunction region with alien materials and destroy 2DEG channel [27].

Despite a decade of effort to improve quality of ohmic contact on AlGaN, the contact's conductivity is still several times higher than those on Si and GaAs. A typical Ti/Al/Mo/Au ohmic contact have around 0.5ohm-mm contact resistance, while most of the GaAs ohmic contacts have less than 0.1 ohm-mm. Several recent efforts have been reported to push contact resistance below 0.3 ohm-mm by exploring on new contact materials and additional surface treatments, but yet have not been mature enough to be widely adopted.[28][29] Large contact resistance adds more loss in the switch's operation. If assuming a typical AlGaN/GaN HFET/MOS-HFET configuration, with 0.5 ohm-mm contact resistance, 300 ohm/sqr channel sheet resistance, and 5 um source-to-drain spacing, ON-state loss (insertion loss) due to contact resistance then accounts for 40% of the total loss, calculated based on equation $R_{ON} = 2R_C + R_{SH}*L_{DS}$.

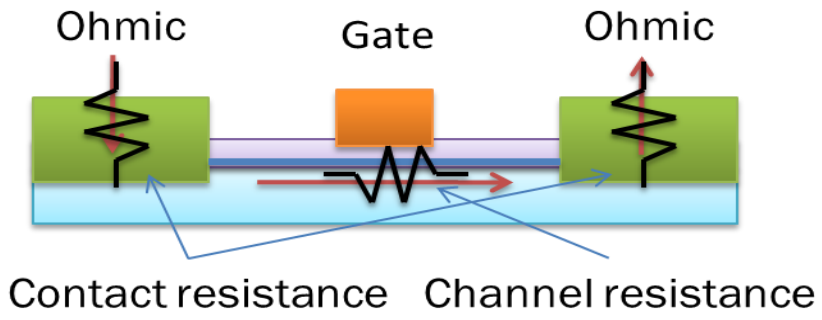

Figure 1.7 Ohmic contacts in III-N HFET Switch

High temperature annealing process also posts limits to fabrication steps and device design. Ohmic contact requires a separate mask, and can only be put in the beginning of fabrication, due to its high temperature requirement.

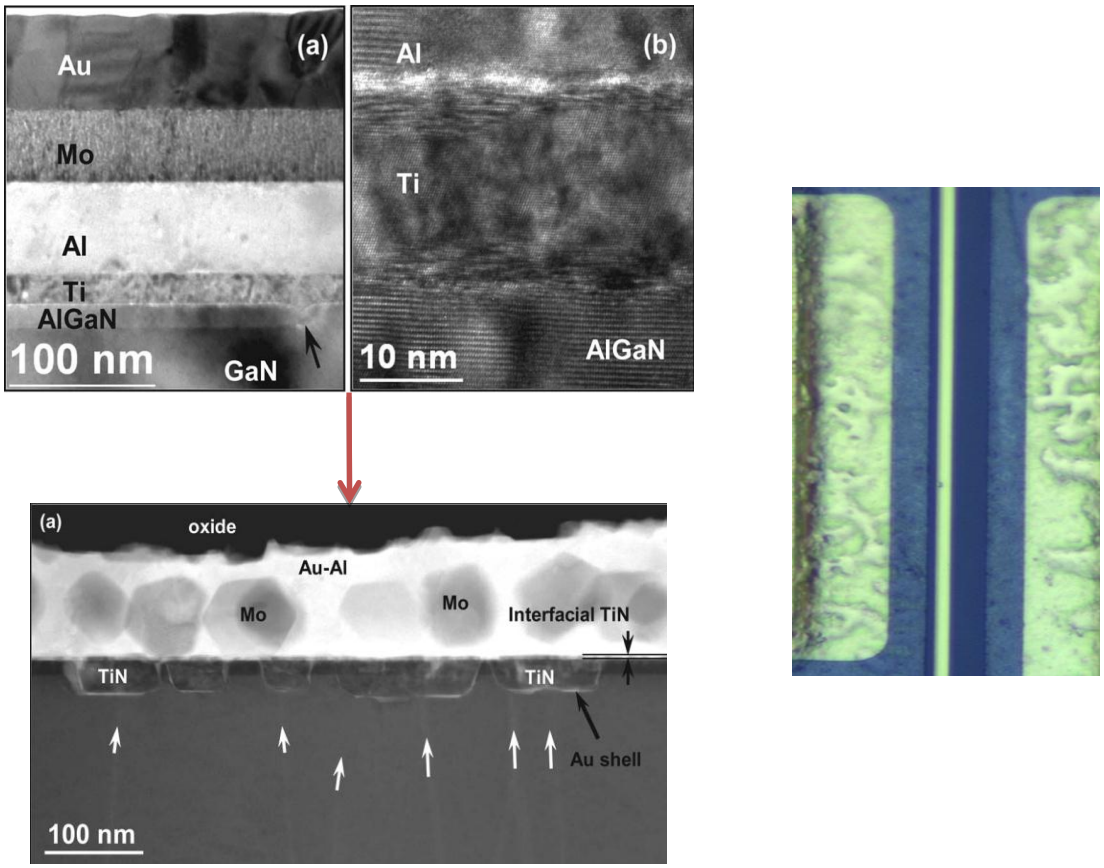

Figure 1.8 (a) TEM image of ohmic contact on AlGaN/GaN before and after annealing [26] (b) zoomed in view of the ohmic contacts

Notable surface roughening and area expanding as the result of high temperature annealing degrades the device's morphological quality, and will see increased RF resistivity and decreased critical breakdown voltage.

The second limitation in AlGaN/GaN HFET based switch design is related to the gate. Low-loss FET RF switches require large device periphery with multi-finger structure, where the alignment of the long and zigzagging gate is a well-known technological challenge. In order to ease the difficulty in processing and maintain high

level of device yield, gate-drain and gate-source spacing is kept above certain “safe” distance to tolerate alignment error, and therefore brings in additional channel length.

The existence of gate introduces source-gate and gate-drain parasitic capacitive coupling between the RF input and output via the metal gate, which limits the isolation [22].

In high-power switches, source-gate and gate-drain spacing needs to be sufficiently high to avoid premature gate breakdown, which also adds to channel length, and therefore leads to higher ON-resistance and higher insertion loss. Sheet resistance of conventional AlGaN/GaN heterostructure is limited by around 300 Ohm/sq value as confirmed by numerous teams working in the field. The channel length is limited by the breakdown voltage. If typically assuming 1 μm gate length and 0.5 μm “safe” distances on each side, with the rest parameters same as those mentioned previously, 24% of the total loss is then related to the existence of gate.

A thin metal gate line is placed in the center of channel between two ohmic contacts in a conventional HFET microwave switch, in order to turn the channel on and off. To reduce insertion loss, device's periphery needs to be expanded dramatically, by employing multifinger layout with channel length as short as a couple of micrometers (very narrow drain-to-source gap). Such design forces gate to be zig-zagging through narrow gap between two sets of ohmic fingers, which makes alignment in gate processing technologically challenging.

In the next chapter a new device type will be introduced in order to overcome these issues with III-N technology.

1.5 Outline of the Dissertation

This dissertation consists of 5 chapters. It can be broadly divided into three main sections. The first segment focuses on the applications of RF switches and RF power limiters and discusses different limitations of existing technology. In the second segment capacitively coupled contacts III-N Heterostructure based varactor is introduced as a solution to the issues of the current technology and its operating mechanism is discussed. The third segment consists of detailed experimental results of this varactor device operating as a RF switch and a RF power limiter.

Chapter 1- Introduction starts with general properties of RF switches and power limiters and their applications. Then different device technologies are compared as RF switch and power limiter applications. Finally III-Nitride HFET technology and its limitations are discussed briefly.

Chapter 2- Capacitively Coupled Contacts (C3) III-N HFET is discussed and C3 varactor is introduced as an improved technology over C3 HFET. Then the varactor operating mechanism as a RF switch and RF power limiter are described and simulation results are validated using experimental data.

Chapter 3-C3 varactor over III-N heterostructure operation as a RF switch is discussed in detail with experimental results. SPST RF switch small and large signal performances along with switching speed are shown in detail.

Chapter 4- C3 varactor over III-N heterostructure operation as a power limiter is discussed in detail with experimental results. RF power limiter loss and limiting power for different dimensions, high power stress and temperature stability of the devices are shown in detail.

Chapter 5- This chapter summarizes the overall results achieved in this dissertation for performance improvement of RF control devices and also presents the future research directions in this field.

CHAPTER 2

INTRODUCTION TO C3 VARACTOR

2.1 Capacitively Coupled Contacts (C3) Based III-N RF Switches

As a solution to the issues degrading performance of the III-N technology due to ohmic contacts ,Capacitively Coupled Contacts or C3 technology was introduced.Unlike power amplifiers, RF switches do not require DC current owing between the input and output ports. This enables more flexibility in switch design. Instead of using ohmic contact to inject RF signal directly into HFET's active region, it can be achieved using capacitive coupling between metal electrodes and the channel beneath, which then eliminates the need of ohmic contacts.[30]

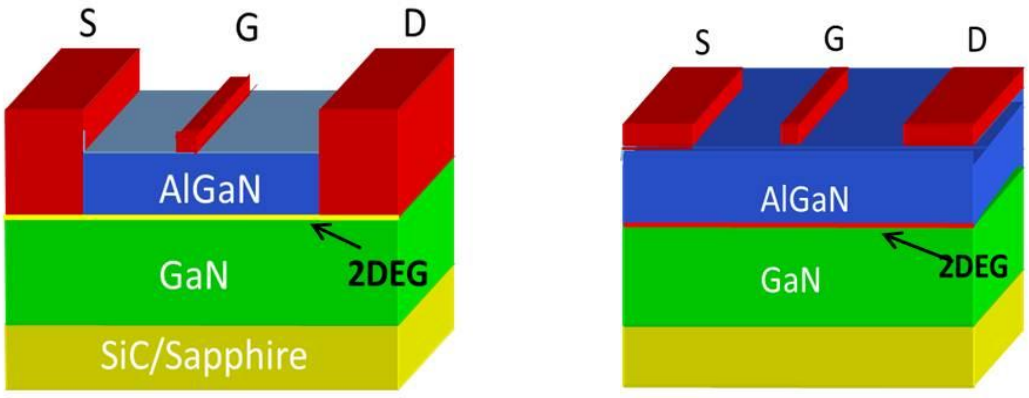

(a) (b)

Figure 2.1 Schematic diagram of a pair of (a)ohmic contacts and (b)capacitively coupled contacts III-N HFET RF switches

Comparison between ohmic and capacitively coupled contacts (C3) is shown in Figure 2.1. A thin dielectric layer (5 - 10 nm) is formed on top of AlGaN before C3 deposition, in order to passivate AlGaN surface and reduce potential leakage current when C3 is under heavy bias voltage. No annealing is needed to form C3, which makes it easy to be integrated into standard metal deposition mask and incorporated into self-aligned process of very fine device designs. No multilayer metal stack is needed as well, compared to ohmic contact, and the choice of material is solely based on metal conductivity, for which Au is the obvious candidate.

The experimental results show that, at high frequencies contact resistance of such C3 is 30% lower than that of a typical ohmic contact. The floating 2DEG channel is modulated according to bias, and through the oscillating movement of free electrons in the channel, the RF signal is passed from one contact to the other.

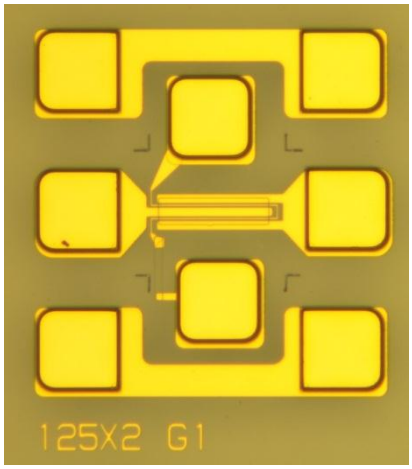

Figure 2.2 C3 HFET switch MMIC

C3 was initially proposed as a simple substitution to more complicated ohmic contact technology. And the first device reported using it was solely based on this purpose. C3-MOSHFET is a C3 version of MOSHFET, and was shown to have advantage in power performance even at relatively low frequencies [31][32]. Simple C3 pair as shown in Figure 2.2 then has the ability to pass or block RF signals based on DC bias applied across it, and becomes a RF switch. Figure 2.3 shows the small signal performance in C3 HFET and regular III-N ohmic contact HFET. The insertion loss in ON state improves significantly in C3 HFET as the loss due to ohmic contacts decreased. The isolation in OFF state also shows comparable results with the regular HFET switch.

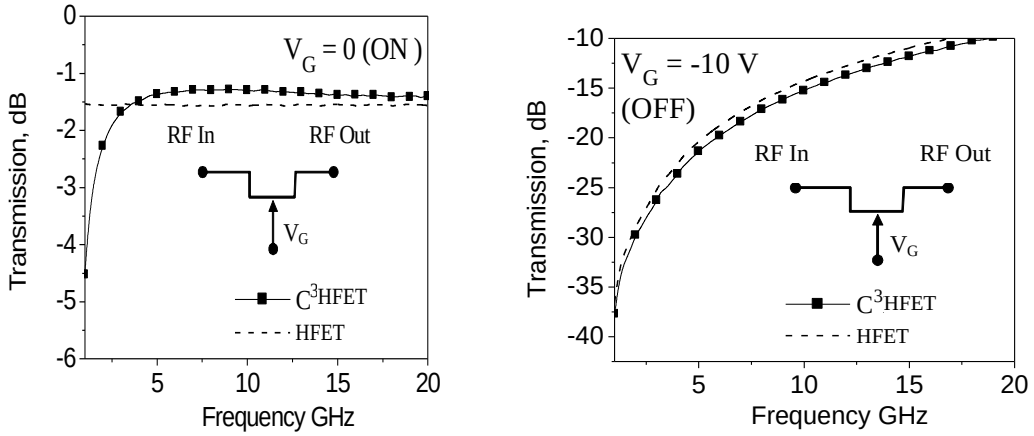

Figure 2.3 (a) Insertion loss and (b) Isolation of C3 III-N HFET RF switch with comparison to ohmic contacts switch

As mentioned earlier, replacing ohmic fingers with C3 ones can solve difficulty in gate alignment, since both C3 and gate can be processed with one mask and self-aligned. Yet, having a metal gate between two fingers takes up extra channel space (additional channel resistance) and posts risks for premature gate breakdown when switching high power signals [33].

Modern systems require yet lower loss, higher power and higher operating frequencies. These goals can hardly be met using existing transistor technology (mainly based on heterostructure field-effect transistors, HFETs) for the above mentioned main reasons. Further performance improvement of RF switches, power limiters and other control devices became inevitable.

To achieve significant performance improvement over that of HFETs, novel type of RF switches and power limiters using novel two-terminal III-Nitride heterostructure varactor with capacitively-coupled contacts (C^3) over low-resistive AlGaN/GaN is introduced as the primary research outcome of this dissertation.

2.2 C3 varactor Operating Mechanism

The novel C3 varactor concept makes this device radically different from traditional HFETs in terms of layout and operating mechanism; it promises improved performance at high frequency range, simplified processing with higher yield and enhanced reliability. At the same time, novel switches based on the varactor are fully compatible with existing III-Nitride HFET technology and can be easily integrated into robust high power MMICs.

The key idea behind C3 design is that, the vast majority of RF control devices do not require the DC current flowing through them and therefore do not need annealed

ohmic contacts to operate. The RF signal injection in the device active region in C3 device is achieved via strong capacitive coupling between metal electrodes and highly-conducting 2D-channel. The higher the operating frequency, the more efficient is the RF signal injection in C3 devices.

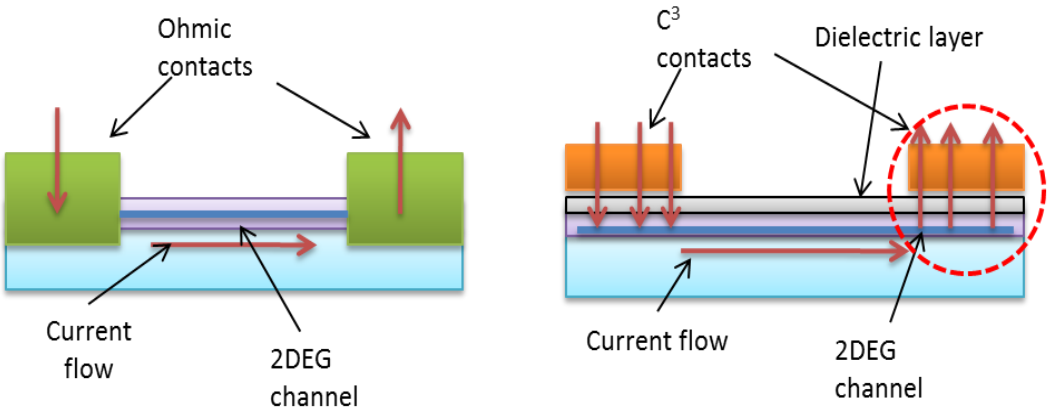

Figure 2.4 Comparison between ohmic and C3 contacts

The varactor shown in Fig. 2.5 consists of two electrodes deposited on top of AlGaN/GaN structure. Optionally, the structure may also incorporate thin dielectric layer below the metal electrodes to further reduce the leakage current. The electrodes form capacitively coupled contacts (C3) with 2DEG channel with low RF impedance at frequencies typically above 2 GHz. [30]

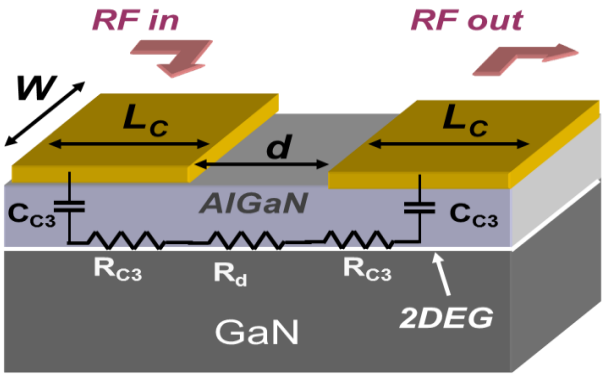

Figure 2.5 The C3 varactor layout with equivalent circuit

C3 varactor has a number of important advantages for RF switching application over HFET devices.

(1) The resistive component of C3 impedance is as low as 1 ohm×mm, smaller than that typically achievable in HFET technology. The capacitive component can be compensated by the switch matching circuit.

(2) C3 varactor has no gate; therefore, the total channel length is more than two times smaller than in the HFET designed for the same breakdown voltage.

(3) C3 varactor has no ohmic contacts; this further increases the breakdown voltage due to much lower edge roughness.

(4) C3 varactor can be controlled using either positive or negative bias polarity.

(5) C3 varactor provides a built-in DC block.

(6) C3 varactor offers high-yield simple and robust anneal-free, alignment-free fabrication technology fully compatible with Power amplifiers and MMICs. The C3 devices can be fabricated using self-aligned process without involving high-temperature contact annealing.

The impedance of C3 varactor is defined by a Series connection of two C3 electrodes and the channel between the contacts. At zero bias, both electrodes have the same impedance. The C3 contact forms an RC-transmission line between the metal electrode and 2DEG channel. The propagation constant γ, the characteristic impedance of the RC line Z_0 and the impedance Z_{C3} of the C3 electrode are given by:

$$\gamma = \sqrt{j2\pi f R_{SH} C_1}; \qquad Z_0 = \frac{1}{W}\sqrt{\frac{R_{SH}}{j2\pi f C_1}} \tag{1}$$

$$Z_{C3} = Z_0 \coth(\gamma L_C) \tag{2}$$

Where f is the operating frequency, R_{SH} is the sheet resistance of the channel, C_1 is the unit-area capacitance between the electrode and the channel, L_C and W are the electrode length and width.

The total varactor impedance at zero bias is therefore

$$Z_V = 2Z_{C3} + R_d, \tag{3}$$

where $R_d = R_{SH} \times d/W$, d is the electrode spacing

At relatively low frequencies, $|\gamma L_C| << 1$, the C3 impedance reduces to that of the series connection of capacitance C_{C3} and equivalent resistance R_{C3}: When the physical length of C3 is sufficiently smaller than its characteristic length according to TL model, the total impedance can be approximated as a series resistor with one-third of the total channel resistance of C3, and a series capacitor with the capacitance equals to a parallel capacitor of the same geometry.

$$C_{C3} \approx C_1 W L_C; \quad R_{C3} \approx R_{SH} L_C/(3W) \qquad (4)$$

The resistive part of the contact impedance and the gap resistance are the main components of the loss introduced by varactor. The capacitive component of the contact impedance can be compensated by external network. Therefore, to achieve low loss, both the gap and the electrode length need to be small enough.

When the voltage across any of the two C3 electrodes exceeds the pinch-off voltage, the 2DEG under the contact depletes and the varactor switches off.

The C3 varactor connected in series into a transmission line, presents low impedance to RF voltage with the amplitude smaller than the turn-off voltage V_{TO}. However when the voltage exceeds V_{TO}, the channel under the reverse-biased electrode depletes, the capacitance drops and the device impedance rapidly increases. This mechanism enables the C3 varactor operation as an efficient RF PL.

When RF voltage amplitude across the device $V_V < V_{TO}$, $V_V = V_L \times |Z_V|/R_L$, where V_L and R_L are the load voltage amplitude and the load resistance. The power limitation occurs when $V_V \approx V_{TO}$. At this point, the corresponding maximum linear load voltage and power are:

$$V_{LM}=V_{TO}\times R_L/|Z_V|; \quad P_{LM} = V_{LM}^2 \big/ (2R_L) \qquad (5)$$

2.3 C3 Varactor Test Structure Design & Fabrication

For initial validation of this novel device concept, a multi-finger C3 varactor test structure having the total width of 500 um with each electrode 2 um long and 50 um wide was designed. The gap between the two electrodes was kept also 2 um.

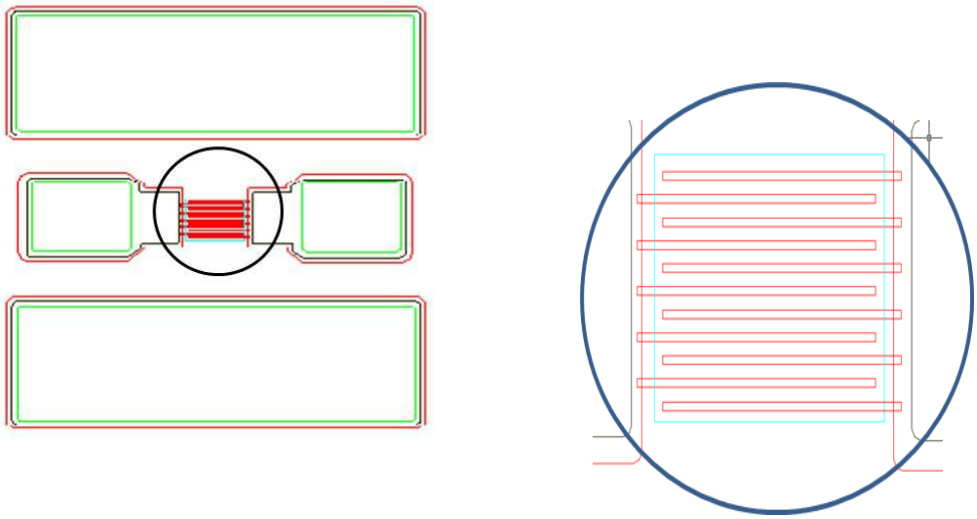

Figure 2.6 Schematic digram of the C3 varactor test element with zoomed in active region

The fabricated[1] C3 varactors have interdigitated structure with 2 um electrode length, 2 um gap and a single finger width 50 um to minimize the effects of the current crowding in metal electrodes The epilayer structure for the varactor was grown on sapphire substrates using MEMOCVD® . A low-doped 20 nm thick $Al_{0.25}Ga_{0.75}N$ barrier was grown over 1.5 um thick i-GaN buffer. The 2DEG sheet resistance was 300 Ohm/Sq. Mesa patterns were formed using RIE. The deposited electrodes were Ni/Au stacks. The

[1] Device fabrication has been done at Sensor Electronic Technology, Inc.

surface was passivated with PECVD deposited 10 nm Si_3N_4 film. The bias resistors of around 2.5 - 5 kOhm have been formed by 3 um wide, 2 - 3 mm long meander shaped lines made of 3 nm thick Pt film. The switch was integrated with CPW formed by Ni/Au metallization over semi-insulating GaN buffer. Compensating inductances (around 0.1 – 0.2 nH) were implemented by locally narrowing the signal lines and increasing the gap in the CPW pattern.

For a varactor with the electrode length and the gap $L_C = d = 2$ um fabricated over AlGaN/GaN heterostructure with 20 nm thick barrier, sheet resistance $R_{SH} \approx 300$ Ohm, it is obtained from (3) and (9) $R_{C3} = 0.2$ ohm×mm, Rd = 0.6 ohm×mm and the total varactor active resistance $R_V = 1$ ohm×mm. The C3 capacitance for the above structure is $C_1 \approx 8$ pF/mm. For comparison, the HFET switch with 2 um source-gate and gate-drain spacing, 0.5 um long gate and 0.5 ohm×mm contact resistance would have the total on-resistance $R_{HFET} = 2.35$ ohm×mm.

The C3 varactor C-V shown in Fig. 2.7 was measured at 1 MHz. The 2 pF value is very close to the geometrical capacitance of two C3's in series. On-wafer small-signal characterization of the C3 varactor was performed with a HP8150C VNA; Power dependencies were measured at 2 GHz.

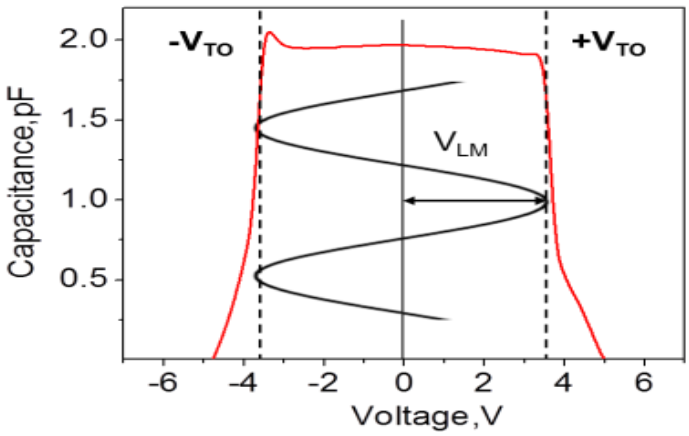

Figure 2.7 Experimental C-V (V_{LM} illustrates the maximum voltage across C3 varactor before power limitation occurs)

2.4 Experimental Validation of C3 Varactor RF Switch Operation

The C3 varactor can be turned off by applying the voltage across any of its contacts exceeding the turn-off voltage V_{TO}, typically around 3 - 5 V for Schottky and 6 – 9 V for metal-insulator-semiconductor (MIS) type contacts.

The turn-off voltage of C3 varactor is approximately the sum of the channel pinch-off voltage ($V_{PO} \approx 2.5$ - 4 V for AlGaN/GaN), and the voltage under the forward-biased Schottky contact $V_{bi} \approx 0.5$- 0.7 V.

In the switch on-state, biasing was kept at zero voltage. In the switch off-state, the control voltage of V_B = +30V was applied to one of the electrodes which turns the device off.

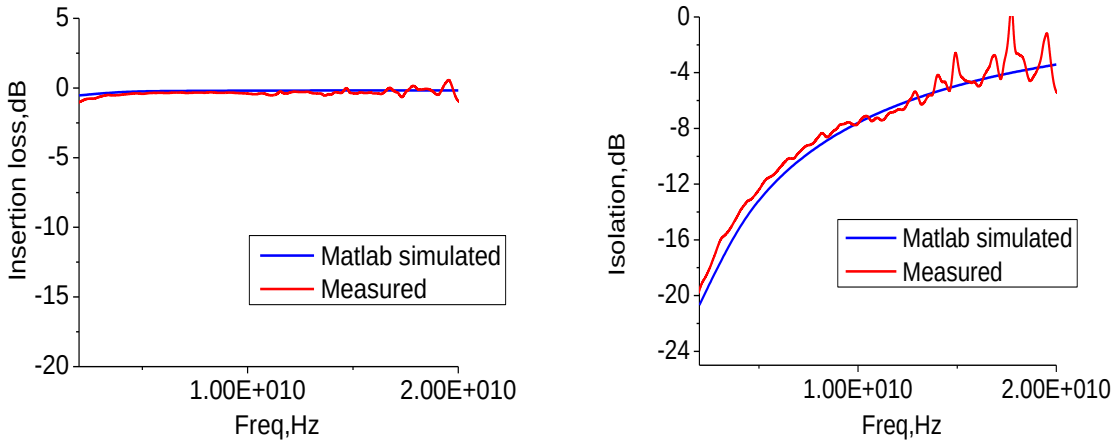

(a) (b)

Figure 2.8 (a) ON state Insertion loss and (b) OFF state Isolation for the RF switch

The experimental results showed very low insertion loss (IL) in ON state, for instance at 15 GHz the IL is less than 0.35 dB. As seen, the experimental results show very close agreement with the MATLAB simulations.

The experimental results are in quite reasonable agreement with the simulation results for OFF state as well.

2.5 Experimental Validation of C3 varactor RF Power Limiter Operation

The fabricated test structure C3 PL shows very small difference between 1 dB compression and saturation powers thus featuring very sharp power limitation. The observed power roll-off beyond the saturation point is believed to be due to self-heating.

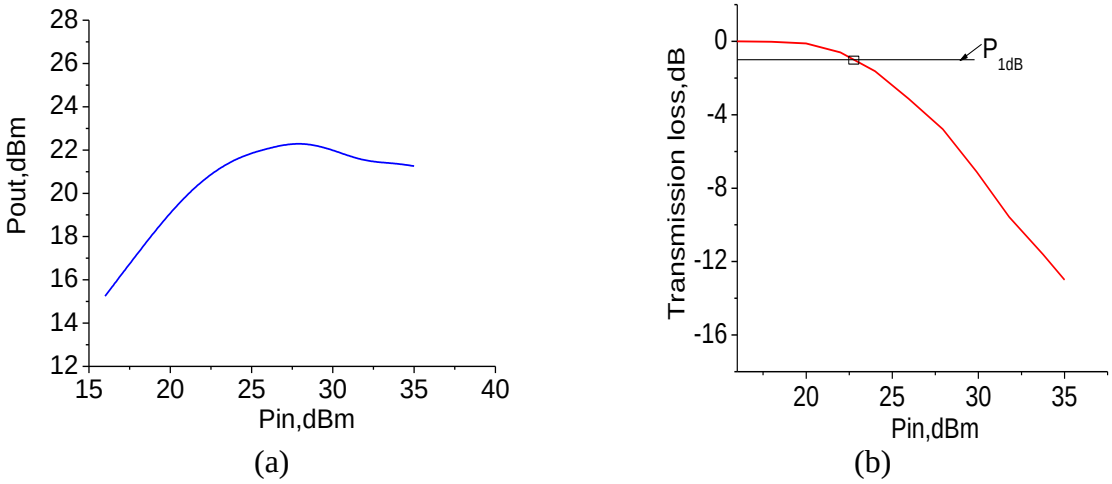

Figure 2.9 (a) Output power and (b) transmission loss of the PL

The power limiter loss measured at 2 GHz also shows reasonable fit with the device width dependence simulation plot

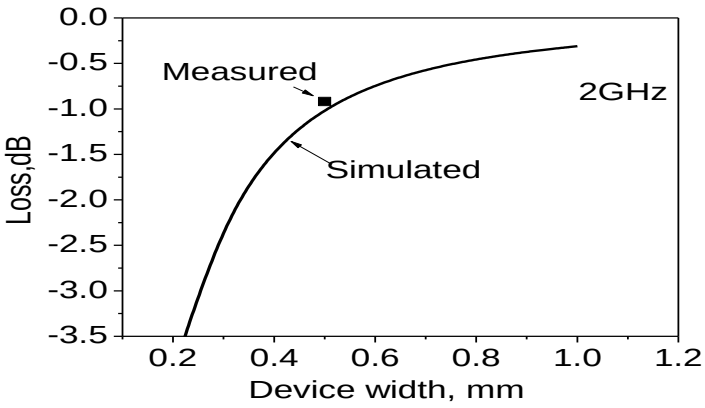

Figure 2.10 C3 PL loss variation with increasing device width

The power limited by the device can be further increased by increasing the width of the device, which proportionally increases the maximum power.

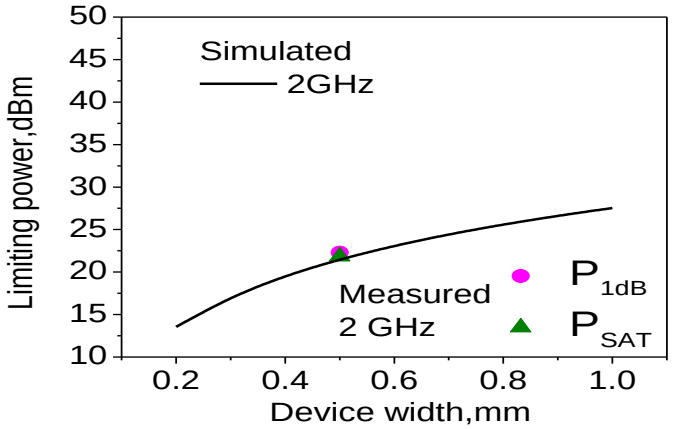

Figure 2.11 C3 PL limiting power variation with increasing device width

The experimental point for the 1 dB power compression and the saturation power as well show excellent agreement with the simulated data.

The next two chapters will elaborately discuss experimental results of this varactor as a SPST RF switch and RF power limiter with varying dimensions.

CHAPTER 3

C3 VARACTOR AS A SPST RF SWITCH

3.1 Introduction

In this chapter low loss RF switch MMIC built using voltage controlled capacitors formed by two Schottky contacts deposited over an AlGaN/GaN heterostructure is demonstrated. Symmetrical structure of the varactor allows for either positive or negative control voltage. Small electrode and spacing size of 2 um ensures a low on-impedance. The fabricated series-shunt switch MMIC shows 0.8 dB insertion loss and 27 dB isolation at 18 GHz and the maximum linear power of 34 dBm at 10 GHz and 38 dBm at 18 GHz (extrapolated from 2 – 10 GHz data). The device does not require contact alignment or annealing, is robust, simple to fabricate, and is well suited for MMICs.

A voltage-controlled capacitor (varactor) formed over 2DEG has been shown to have high capacitance on/off ratio up to microwave frequencies[34][35]; it was also suggested to be a promising switching device [37][38], however no RF switches based on III-Nitride varactors have ever been demonstrated.

The varactor shown in Fig. 3.1 consists of two electrodes deposited on top of AlGaN/GaN or dielectric/AlGaN/GaN structure. The electrodes form capacitively coupled contacts (C3) with 2DEG channel with low impedance at RF frequencies, typically above 2 GHz. The C3 varactor can be turned off by applying the voltage across any of its contacts exceeding the pinch-off voltage, typically around 3 -4 V for Schottky

and 6 – 9 V for MIS type contacts. Just as heterostructure field-effect transistor (HFET), C3 varactor does not consume significant DC bias power; in addition, as mentioned earlier in chapter 2, it offers several important advantages as an RF switching device: (1) it has no gate, so the total channel length is more than two times smaller than in HFET with the same source – gate and gate-drain spacing and, hence, about the same breakdown voltage; (2) it has no ohmic contacts; and, therefore, does not require annealing and the need to align the gate. This further increases the breakdown voltage due to lower edge roughness; (3) it can be controlled using either positive or negative bias polarity.

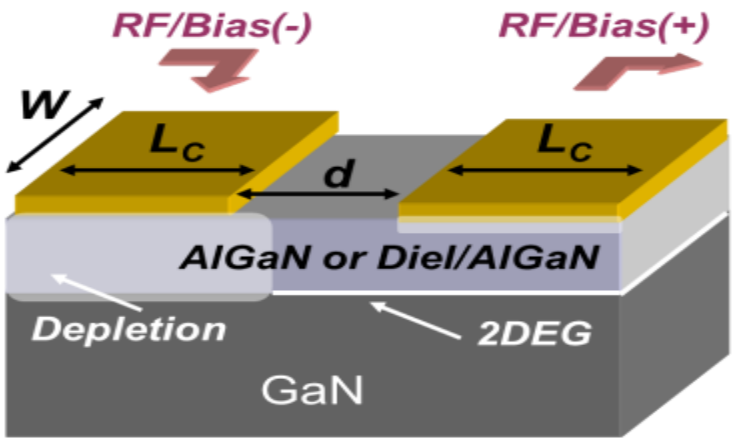

Figure 3.1 C3 varactor RF switch layout

Here, a low-loss broadband 2 – 20 GHz series-shunt RF switch MMIC using the C3 AlGaN/GaN varactor is demonstrated.

3.2 Switch Design and Fabrication

As already discussed in chapter 2, the impedance of this C3 varactor is a series connection of two electrodes and the channel between the contacts. At zero bias, both electrodes have the same impedance. The contact forms an RC-transmission line between the metal electrode and 2DEG channel. For the convenience of understanding the design method the equations mentioned in chapter 2 are stated again. The propagation constant γ, the characteristic impedance of the RC line Z_0 and the impedance Z_{C3} of the C3 electrode are given by (see, e.g. [9]):

$$\gamma = \sqrt{j2\pi f R_{SH} C_1}; \; Z_0 = \frac{1}{W}\sqrt{\frac{R_{SH}}{j2\pi f C_1}} \qquad (6)$$

$$Z_{C3} = Z_0 \coth(\gamma L_C) \qquad (7)$$

where f is the operating frequency, R_{SH} is the sheet resistance of the channel, C_1 is the unit-area capacitance between the electrode and the channel, L_C and W are the electrode length and width. In Eq. (1) we ignored the shunting conductance corresponding to leakage current; at microwave frequencies, it is typically much smaller than the capacitive admittance.

The total varactor impedance at zero bias is therefore

$$Z_V = 2Z_{C3} + R_d; where\, R_d = R_{SH} d / W, \qquad (8)$$

where d is the electrode spacing.

At relatively low frequencies, $|\gamma L_C| << 1$, the C3 impedance Z_{C3} reduces to that of the series connection of capacitance C_{C3} and equivalent resistance R_{C3}[37]:

$C_{C3} \approx C_1 W L_C$; $R_{C3} \approx R_{SH} L_C/(3W)$ (9)

The resistive part of the contact impedance and the gap resistance are the main components of the loss introduced by varactor. The capacitive component of the contact impedance can be compensated by external network.

The approximation (9) for this device holds up to around 30 GHz. The C3 capacitance for the above structure is $C_1 \approx 8$ pF/mm. When the voltage across any of the two C3 electrodes exceeds the pinch-off voltage, the 2DEG under the contact depletes and the varactor capacitance decreases to a low off-state value C_{OFF}. The C_{OFF} capacitance of the pinched off electrode was experimentally found to be around 0.15 pF/mm. As seen, the C_{OFF} is more than 50 times smaller than that in the on-state.

The RF switch for this work was designed using series-shunt layout (Fig. 3.2); series and shunt C3 varactors have multi-finger structure with 2 um electrode length, 2 um gap and single finger width W1 = 50 um to minimize the effects of the current crowding in metal electrodes [40]. The width of the series and shunt varactors, W_{SER}= W_{SHT} = 10×W1 = 0.5 mm, was optimized in MATLAB using Eqs. (6-8) and the off-state capacitance C_{OFF} = 0.15 pF/mm to simultaneously achieve minimal loss with isolation of at least 25 dB at 18 GHz.

The optimization process carried out to find out the ultimate combination of series and shunt device dimensions is shown below (Fig. 3.2 and Fig. 3.3).The insertion loss and isolation were simulated over series device widths for different shunt device dimensions to find out the best match.

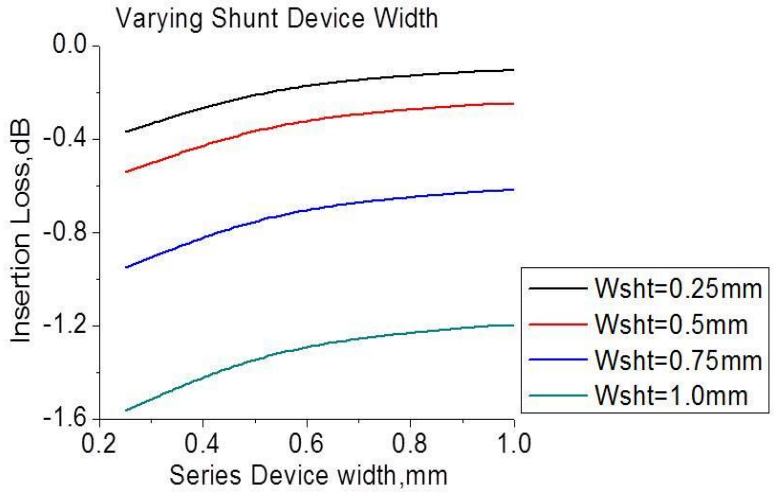

Figure 3.2 Simulated Insertion loss with varying series device width for different shunt device dimensions

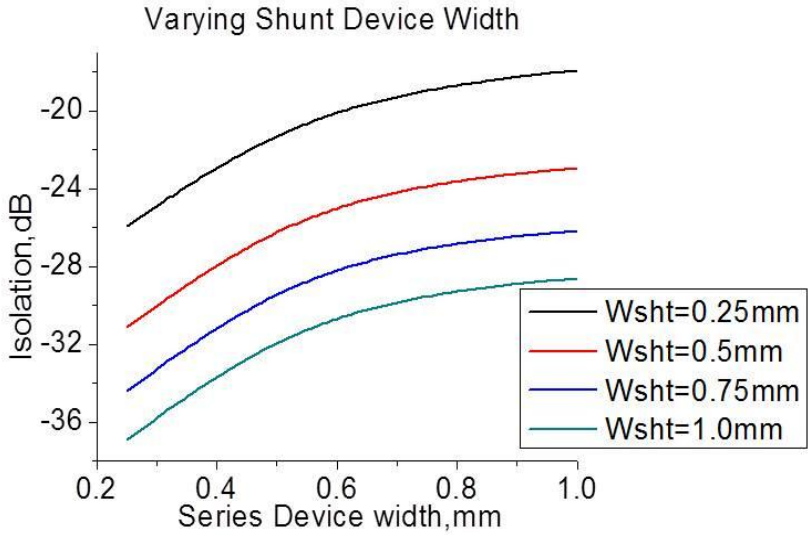

Figure 3.3 Simulated Isolation with varying series device width for different shunt device dimensions

A segment of the the Matlab codes used for the switch optimization is shown in Fig. 3.4

```
%S-D spacing um
Lsd=2;
% Series device width, mm;
Wsrs=0.5;
% Shunt device width, mm ;
Wsht=0.5;
% Off capacitance per 1 mm
Coff1=0.15e-12;
%Contact length, um
Lcum=2;
Lc=Lcum*1e-4; %contact length in cm
% C3 capacitance per 1 cm2
eps0=8.85e-14;
epsb=9; %barrier eps
%epsd=3.9; %dielectric eps
db=150e-8; %barrier thickness, cm
%dd=100e-18; %ZERO dielectric thickness, cm
Cb1=eps0*epsb/db; %barrier capacitance per cm2
%Cd1=eps0*epsd/dd; %dielectric capacitance per cm2
%C1bd=1/(1/Cb1+1/Cd1);
%**********************
% ON resistance
% C3 ON impedance
%**** at resonant frequency******
%C1=C1bd; %C3 capacitance per unit area
C1=Cb1;
Z1C3r=Rsh;
Y1C3r=i*om*C1;
ZOr=sqrt(Z1C3r./Y1C3r);
Gamr=sqrt(Z1C3r*Y1C3r);
ZC31r=ZOr.*coth(Gamr*Lc); %C3 impedance per unit width in Ohm*cm;
% Two C3 contacts in series impedance
ZC3srs=ZC31r/(0.1*Wsrs);
ZC3sht=ZC31r/(0.1*Wsht);

%ZLsrsr=-i*imag(ZC3srsr); %resonant inductance impedance to compensate series C3 c
```

Figure 3.4 Matlab codes for switch design

After that, small inductances have been added in series with both series and shunt varactors to compensate the capacitive component of the C3 impedance.

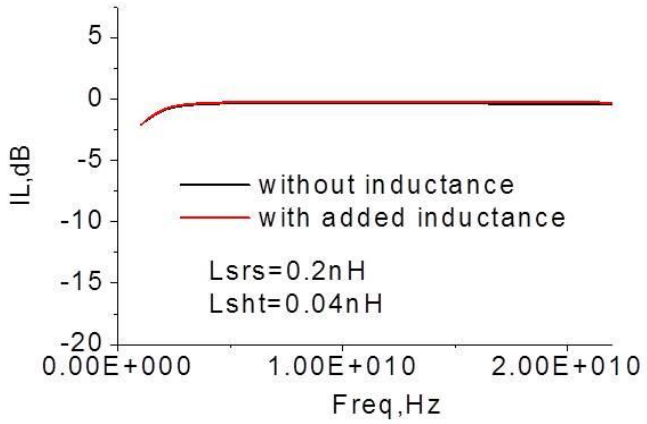

Figure 3.5 Simulated Insertion loss over varying frequency with and without added inductance

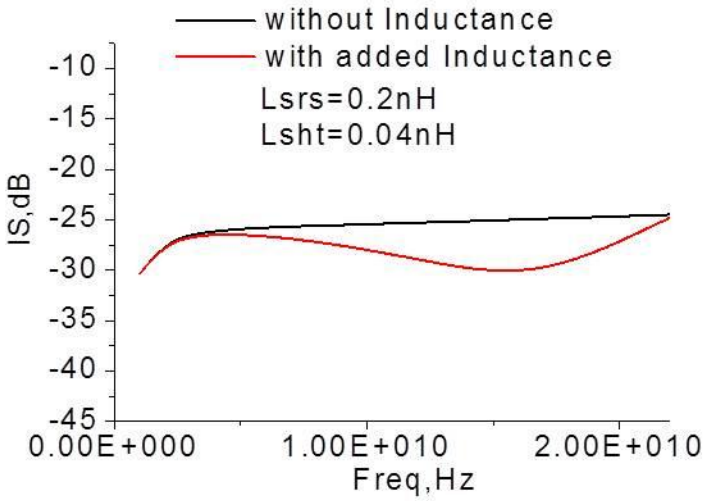

Figure 3.6 Simulated Isolation over varying frequency with and without added inductance

The epilayer structure for the switch was grown[2] on sapphire substrates using MEMOCVD® [41]. A low-doped 20 nm thick $Al_{0.25}Ga_{0.75}N$ barrier was grown over 1.5 um thick i-GaN buffer. The 2DEG sheet resistance was 300 ohm/Sq. Mesa patterns were formed using RIE. Schottky electrodes were Ni/Au stacks. The surface was passivated with PECVD deposited 10 nm Si_3N_4 film. The leakage current was in the range of 2 – 10 uA at 30 V. The bias resistors of 2.5 - 5 kOhm have been formed by 3 um wide, 2 - 3 mm long meander shaped lines made of 30 nm thick Cr film. The switch was integrated with CPW formed by Ni/Au metallization over semi-insulating GaN buffer.

Compensating inductances (around 0.1 – 0.2 nH) were implemented by locally narrowing the signal lines and increasing the gap in the CPW pattern.

[2] Device fabrication has been done at Sensor Electronic Technology, Inc.

Fig.3.7 shows the layout of series-shunt SPST switch and CCD image of the RF switch MMIC is shown in Fig. 3.8.

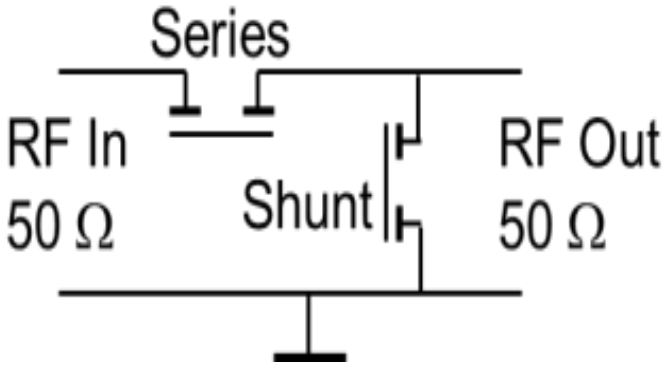

Figure 3.7 Series-shunt MMIC layout

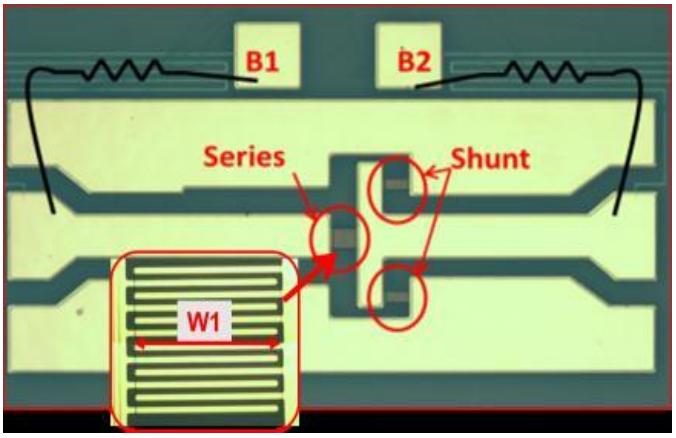

Figure 3.8 RF switch CCD image with the multi-finger C3 region zoomed-in

3.3 Results and Discussion

The C-V characteristics of 500 um wide C3 device has been tested at 1 MHz; the results are shown in Fig.3.9

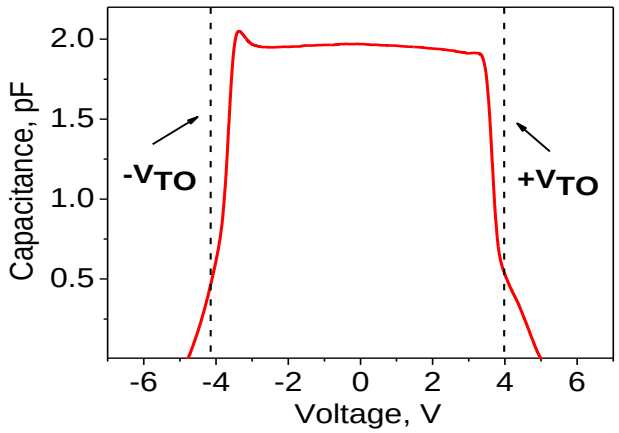

Figure 3.9 Experimental C-V for C3 varactor RF switch

On-wafer small-signal characterization of the switch MMICs was performed with a HP8150C VNA. In the switch on-state, the control voltage of V_B = +30V was applied to both input and output CPW lines. This biasing kept the series device at zero voltage (i.e., in the on-state) and the shunt device at 30 V bias (i.e., in the off-state). In the switch off-state, the bias on the output CPW line was turned to zero, which turns the series device into the off state and the shunt device into the on-state. The measured and simulated small-signal characteristics of C3 varactor switch MMIC are shown in Fig. 3.10 and 3.11

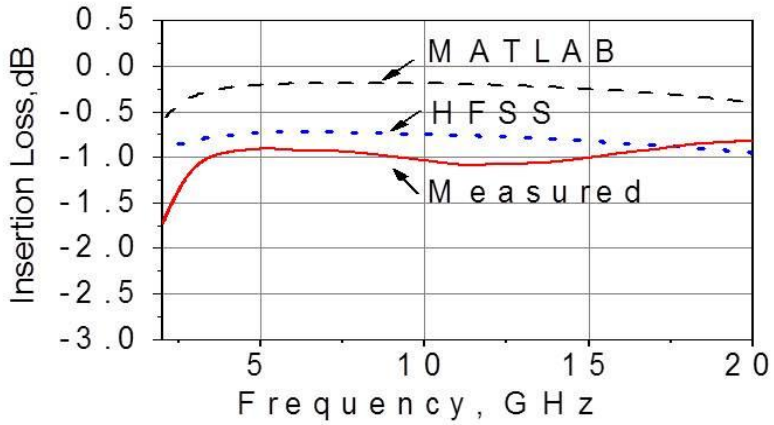

Figure 3.10 Solid lines: Insertion loss of the C3 switch MMIC; dashed – MATLAB, dotted – HFSS simulations

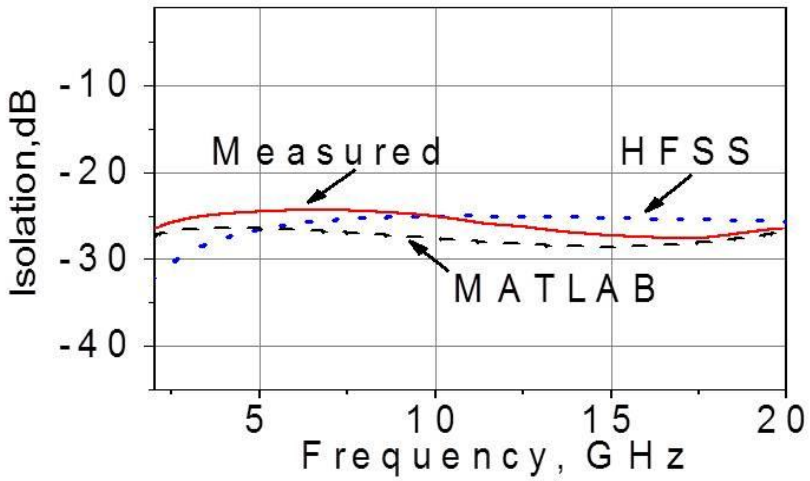

Figure 3.11 Solid lines: Isolation of the C3 switch MMIC; dashed – MATLAB, dotted – HFSS simulations

As seen from Fig. 3.10, the developed switch shows low loss of less than 1.2 dB in a broad frequency range 4 – 20 GHz. At 18 GHz, the insertion loss is 0.8 dB. The loss expected from MATLAB simulations was about 0.5 – 0.7 dB lower than the measured one. It was speculated that the difference is coming from the CPW loss and imperfect

capacitance compensation by the CPW inductance. To verify this speculation, HFSS simulations were performed using the same C3 device characteristics as in MATLAB. As seen, the HFSS results show very close agreement with the experimental data. The obtained C3 switch loss compares favorably with the reported 18 - 20 GHz results, e.g. 1.5 dB for GaN HFET [42] or 2 dB for ferrite varactor switch [43]. The effect of biasing resistors on switch loss was negligible as confirmed by biasing the switch through the bias-Ts connected directly to RF probes.

In the off state, the isolation is around 25 dB in a broad frequency range. The isolation at 18 GHz is 27 dB. The experimental results are in good agreement with the simulations.

The maximum power handled by C3 switch is limited by the following mechanism (please refer to Fig. 3.9). When the series C3 varactor is in the on state, the RF voltage amplitude across the device, $V_V = V_L \times |Z_V|/R_L$, where V_L and R_L are the load voltage amplitude and the load resistance. The power limitation occurs when the amplitude V_V reaches the device turn-on voltage V_{TO}: $V_V \approx V_{TO}$. At this point, the corresponding maximum linear load voltage and power are:

$$V_{LM} = V_{TO} \times R_L/|Z_V|; \qquad P_{LM\_SER} = \frac{V_{LM}^2}{2R_L} \qquad (10)$$

The C3 varactor impedance Z_V is frequency dependent. Therefore, we simulated the frequency dependence of the maximum power given by Eq. (10) using the varactor model described by Eqs. (1 – 3), the experimental value of the turn-on voltage, V_{TO} = 4V and R_L = 50 ohm. For the shunt device in the off state, the power limitation occurs when

the voltage amplitude reaches the value of $|V_B| - |V_{TO}|$. The maximum load power limited by the shunt device:

$$P_{LM\_SHT} = \left(|V_B| - |V_{TO}|\right)^2 / (2R_L) \qquad (11)$$

Fig. 3.12 shows the maximum linear switching powers limited by series and shunt devices obtained from Equations (5, 6). The 1dB compression power has been measured at 2, 5.8 and 10 GHz. The 2 and 10 GHz 1 dB power compression points in Fig. 3.7 show excellent agreement with the simulated data. At 5.8 GHz the maximum available power of +24 dBm was not sufficient to cause the power compression; this is indicated by arrow up in Fig. 3.7. To further confirm that the measured 1 dB compression is caused by the series device, we measured the power dependence of a single C^3 varactor identical to that used in the switch MMIC at 2 GHz. The obtained P_{1dB} value was exactly the same as for the switch MMIC (Fig. 3.13).

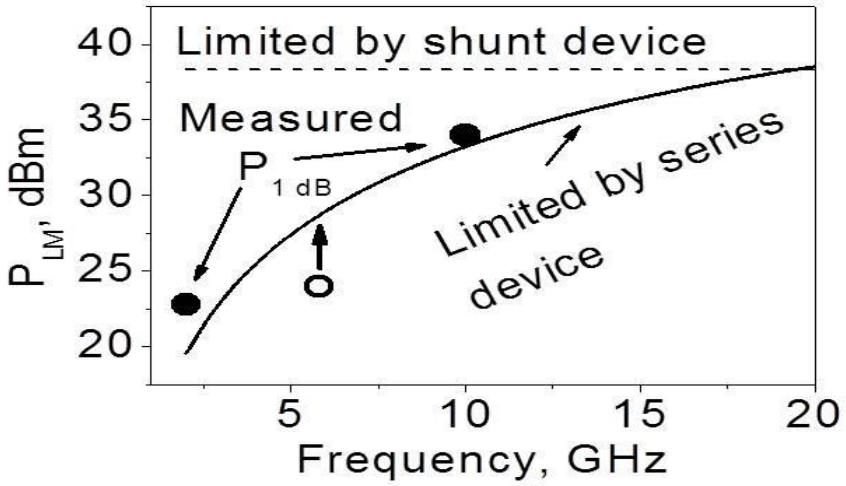

Figure 3.12 Measured (symbols) and simulated (line) maximum switching power of series – shunt C^3 switch

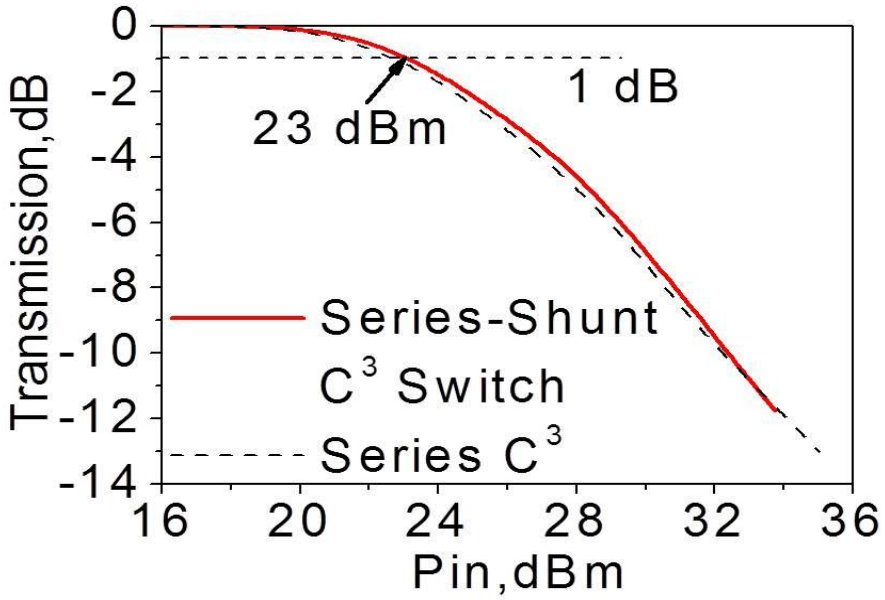

Figure 3.13 Power compression in series-shunt switch compared to series device

The power limited by the series device can be further increased by increasing the width of the series device. The power limited by the shunt device can be further increased by increasing the bias. Maximum bias voltage is limited by the varactor breakdown. For our devices, the breakdown voltage of V_{BD} = 95 V was measured. Therefore, the optimal bias for maximum RF power is $(V_{BD} - V_{TO})/2 \approx 45.5$ V. The corresponding maximum power is $P_{LM\_SHT} \approx 43$ dBm. Note that, for the HFET with the same 2 um gate – drain spacing fabricated from similar epitaxial structure, the breakdown voltage was lower: 45 – 50 V.

The response time of this RF switch was also measured. The pulsed control voltage was generated using HP 8011A pulse generator and switching response was observed using a Tektronix TDS 2022C oscilloscope. Fig. 3.14 shows the block diagram of the experimental set up for the switching response measurement.

Fig. 3.15 and Fig. 3.16 show response time for a schottky varactor switch and a switch with a 10 nm dielectric layer on top.

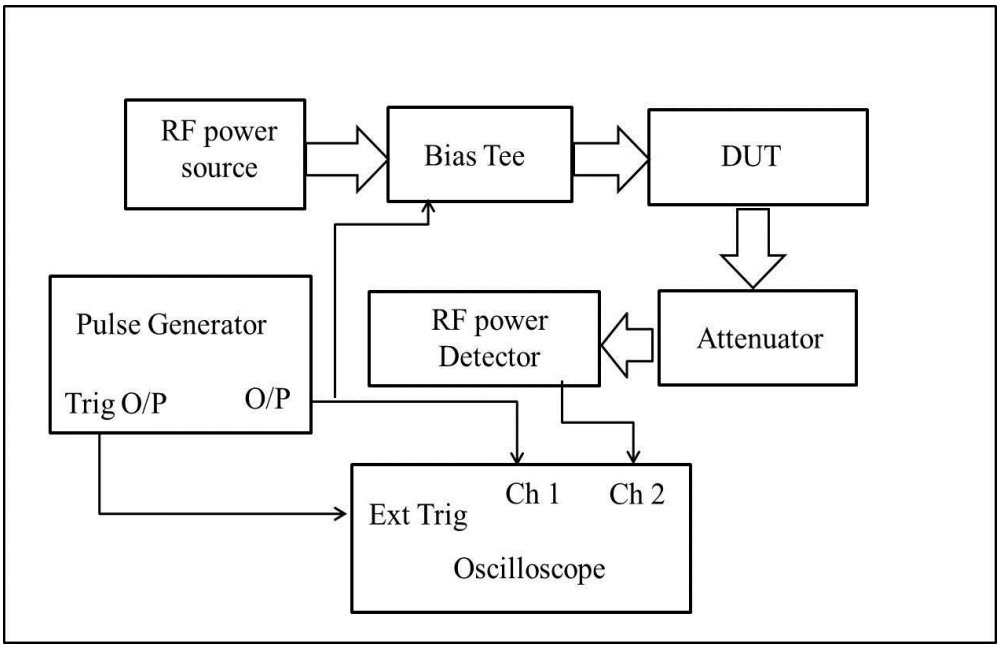

Figure 3.14 Block diagram of switching time measurement set up

The RF signal was applied at 2 GHz frequency and the signal amplitude was 0 dBm. The pulsed voltage amplitude was applied in the range from 10-15V.The switching speed was found to be in the range of 500-800ns for both type of switches which is very fast compared to other device types such as 200-3000 us for thermal/magnetic MEMS switches[44].

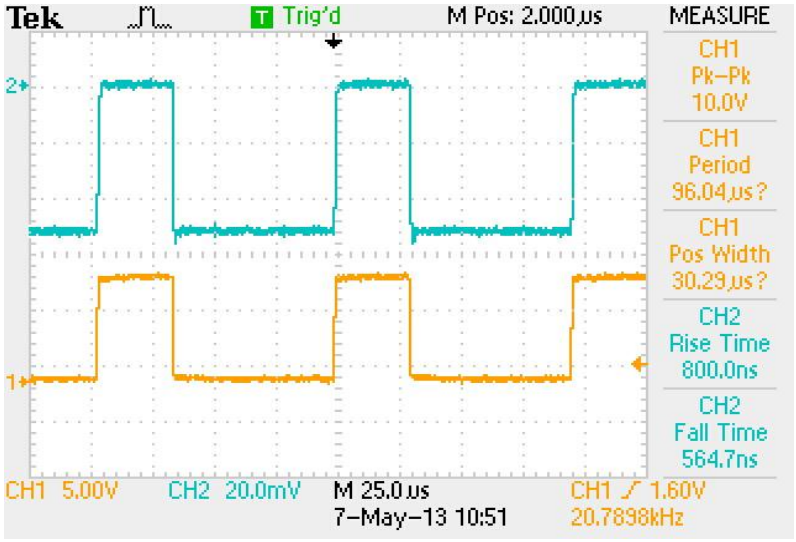

Figure 3.15 Switching time of Schottky C3 varactor Switch; yellow line-applied pulsed control voltage; blue line-Turn on(fall time) and Turn off(rise time) times

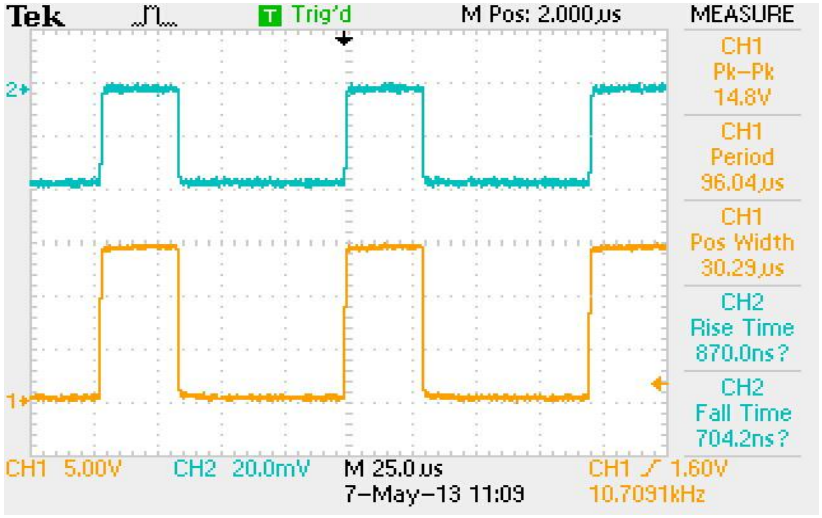

Figure 3.16 Switching time of a C3 varactor Switch with dielectric layer; yellow line-applied pulsed control voltage; blue line-Turn on(fall time) and Turn off(rise time) times

3.4 Conclusions

The demonstrated novel RF switch MMIC with III-Nitride C3 varactors uses simple and robust planar, alignment - and anneal - free fabrication technology. At 18 GHz, the fabricated switch exhibits 0.8 dB loss and 28 dB isolation with breakdown voltage of 95 V for the device with the 2 um spacing. The maximum RF power at 10 GHz is +34 dBm and extrapolated maximum power at 18 GHz is +38 dBm[45][46].The switching time was also found to be in the ns range. The demonstrated switch is fully compatible with III-Nitride HFETs or MISHFETs and has a great potential for high-performance MMICs.

CHAPTER 4

C3 VARACTOR AS A RF POWER LIMITER

4.1 Introduction

In this chapter low loss RF power limiter built using voltage controlled capacitor formed by two planar Schottky contacts deposited over an AlGaN/GaN heterostructure is demonstrated. Symmetrical structure of the varactor enables dual-polarity voltage clamping. Small electrode size and electrode spacing of 2 um ensures a low impedance and low loss. Varying the varactor width in the range 0.25 – 1 mm allows tuning the limitng powers in the range 17 – 40 dBm, also dependent on the operating frequency. The small-signal loss at 10 GHz is 0.2 - 0.67 dB. The varactor structure fabrication does not require gate alignment or annealing; the device is robust and fully compatible with MMICs; it also provides the DC block with around 95 V breakdown. The PL operation in the temperature range 25^{o}C – 200^{o}C without significant parameter degradation was demonstrated. Power limiter CW stress during 100 hrs at 24 dBm revealed no performance degradation[47][48].

As discussed in previous chapters, III-Nitride based heterostructures open tremendous opportunities for microwave control device technology due to the record high sheet electron density in the 2D channel, extremely low channel resistance, high breakdown field, excellent temperature stability and radiation hardness.

Here, a novel type of the RF PL using III-Nitride varactor with capacitively-coupled contacts (C3) is shown.

The C3 varactor shown in Fig. 4.1 consists of two electrodes deposited on top of an AlGaN/GaN or structure. C3 electrodes allow for efficient RF signal injection into the 2DEG channel with low equivalent impedance at high frequencies (above around 2 GHz).

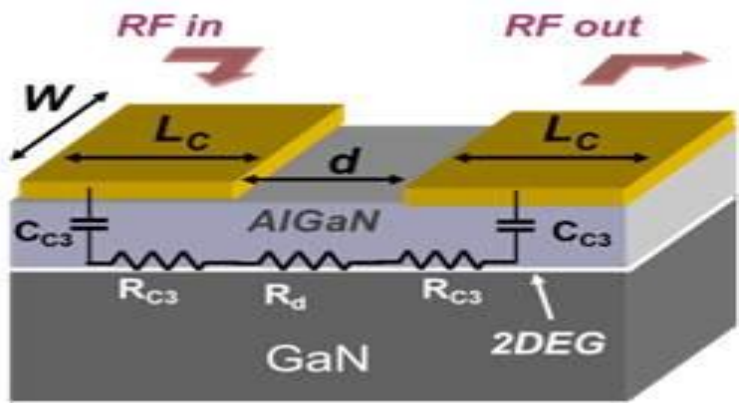

Figure 4.1 Schematic layout of the C3 varactor PL

The C3 varactor connected in series into a transmission line, presents low impedance to RF voltage with the amplitude smaller than the turn-off voltage V_{TO}, Fig. 4.2. However when the voltage exceeds V_{TO}, the channel under the reverse-biased electrode depletes, the capacitance drops and the device impedance rapidly increases.

As the off-capacitance was experimentally found to be around 0.15 pF/mm, which is more than 50 times smaller than that in the on-state, this mechanism enables the C3 varactor operation as an efficient RF PL. C3 varactor offers a simple planar structure fully compatible with MMICs.

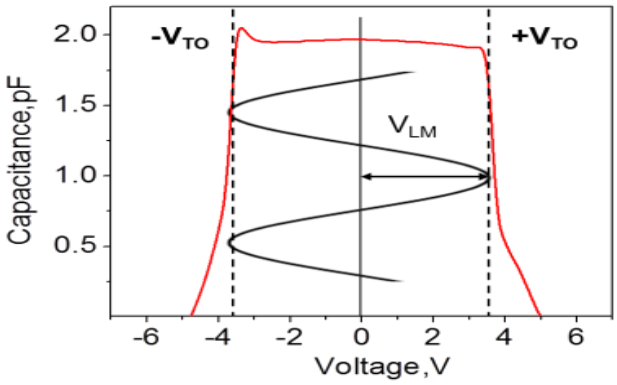

Figure 4.2 Experimental C-V of the varactor PL; VLM illustrates the maximum voltage across C^3 varactor before power limitation occurs.

4.2 PL Design and Fabrication

The impedance of C3 varactor, just as mentioned for the RF switch in Chapter 3, is defined by a series connection of two C3 electrodes and the channel between the contacts. At zero bias, both electrodes have the same impedance. The C3 contact forms an RC-transmission line between the metal electrode and 2DEG channel with the propagation constant γ and the characteristic impedance of the RC line Z_0 and the impedance Z_{C3} of the C3 electrode are given by:

$$\gamma = \sqrt{j 2\pi f R_{SH} C_1}; \qquad Z_0 = \frac{1}{W}\sqrt{\frac{R_{SH}}{j 2\pi f C_1}} \tag{12}$$

$$Z_{C3} = Z_0 \coth(\gamma L_C) \tag{13}$$

Where f is the operating frequency, R_{SH} is the sheet resistance of the channel, C_1 is the unit-area capacitance between the electrode and the channel, L_C and W are the electrode length and width (Fig.4.1).

The varactor impedance is therefore,

$$Z_V = 2Z_{C3} + R_d\,, \qquad (14)$$

The C3 capacitance for the above structure is $C_1 \approx 8$ pF/mm as found in chapter 3. When RF voltage amplitude across the device $V_V < V_{TO}$, $V_V = V_L \times |Z_V|/R_L$, where V_L and R_L are the load voltage amplitude and the load resistance. The power limitation occurs when $V_V \approx V_{TO}$. At this point, the corresponding maximum linear load voltage and power are:

$$V_{LM} = V_{TO} \times R_L/|Z_V|; \qquad P_{LM} = V_{LM}^2/(2R_L) \qquad (15)$$

A segment of the the matlab codes used for the PL design simulation is shown in Fig. 4.3

```
4
5       %C3 series power limiter
6       %
7 -     clear all;
8
9 -     fGO=5; %operating frequency
10 -    fop=fGO*1e9;
11 -    om=2*pi*fop;
12 -    RL=50; %Load impedance
13      %C3 contact pinch-off voltage
14 -    Vpo=3.5;
15      %Sheet resistance
16 -    Rsh=300;
17      %S-D spacing um
18 -    Lsd=2;
19      % Series device width, mm;
20 -    arrWsrs=0.2:0.1:1;
21      % Off capacitance per 1 mm
22 -    Coff1=0.15e-12;
23      %Contact length, um
24 -    Lcum=2;
25 -    Lc=Lcum*1e-4; %contact length in cm
26      % C3 capacitance per 1 cm2
27 -    eps0=8.85e-14;
28 -    epsb=8.9; %barrier eps
29 -    epsd=3.9; %dielectric eps
30 -    db=230e-8; %barrier thickness, cm
31 -    dd=100e-18; % dielectric thickness, cm
32 -    Cb1=eps0*epsb/db; %barrier capacitance per cm2
33 -    Cd1=eps0*epsd/dd; %dielectric capacitance per cm2
34 -    C1bd=1/(1/Cb1+1/Cd1);
35      %C1bd=Cb1; %Schottky only, no dielectric
36      %**********************
37 -    for msrs=1:length(arrWsrs)
38 -        Wsrs=arrWsrs(msrs);
39
```

Figure 4.3 Matlab codes for PL design

The turn-off voltage of C3 varactor is approximately the sum of the channel pinch-off voltage ($V_{PO} \approx 2.5$ - 4 V for AlGaN/GaN), and the voltage under the forward-biased Schottky contact $V_{bi} \approx 0.5$- 0.7 V.

The C3 varactors fabricated in this work have interdigitated structure with 2 um electrode length, 2 um gap and a single finger width 50 um to minimize the effects of the current crowding in metal electrodes [40]. The total width of varactors ranged from 0.25 to 1 mm. The epilayer structure was grown[3] on sapphire substrates using MEMOCVD®. A low-doped 20 nm thick $Al_{0.25}Ga_{0.75}N$ barrier was grown over 1.5 um thick i-GaN buffer. The 2DEG sheet resistance was 300 ohm/Sq and $V_{TO} \approx 3.5$ V. The mesa patterns were formed using RIE. The deposited electrodes were Ni/Au stacks. The surface was passivated with PECVD deposited 10 nm Si_3N_4 film.

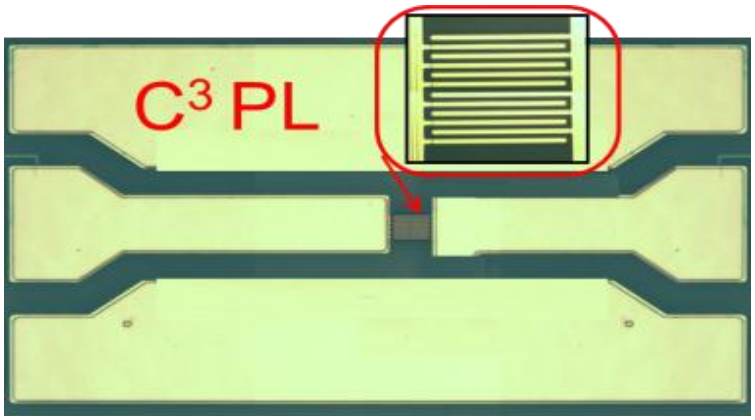

Figure 4.4 The C3 PL MMIC image

[3] Device fabrication has been done at Sensor Electronic Technology, Inc.

4.3 Results and Discussion

The C3 varactor C-V shown in Fig. 4.2 was measured on 0.5 mm device at 1 MHz. The 2 pF value is very close to the geometrical capacitance of two C3's in series. On-wafer small-signal characterization of the C3 PL was performed with a HP8150C VNA, with achieved loss as low as 0.2 dB for 1mm wide PL and good agreement with simulated data of Fig.4.6. Solid lines in Fig. 4.6 show the dependencies of RF PL loss and in Fig 4.7 show limiting power on the width W of the C3 varactor simulated using (11 –14), the C3 data specified above and V_{TO} = 3.5 V.Fig. 4.5 show the block diagram of the experimental set up for the large signal measurement.

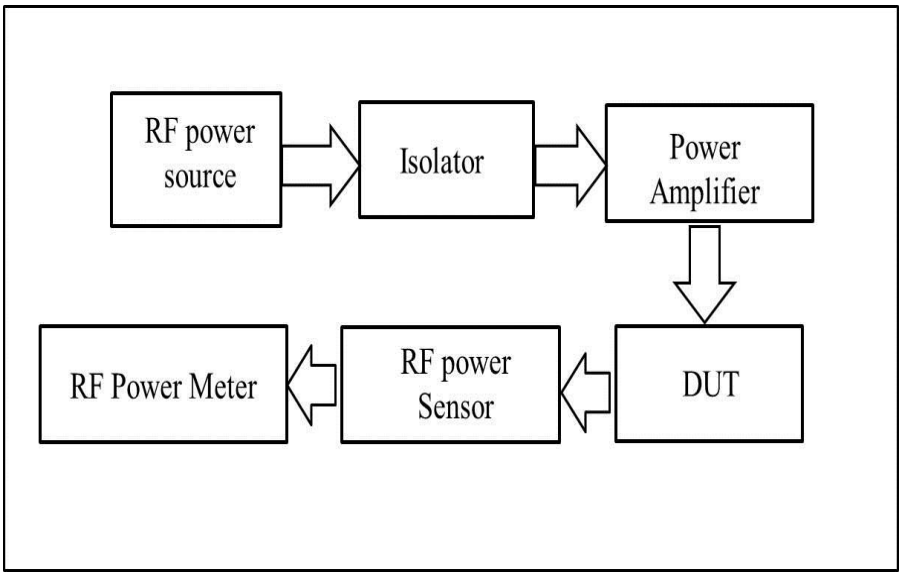

Figure 4.5 Block diagram of large signal measurement set up

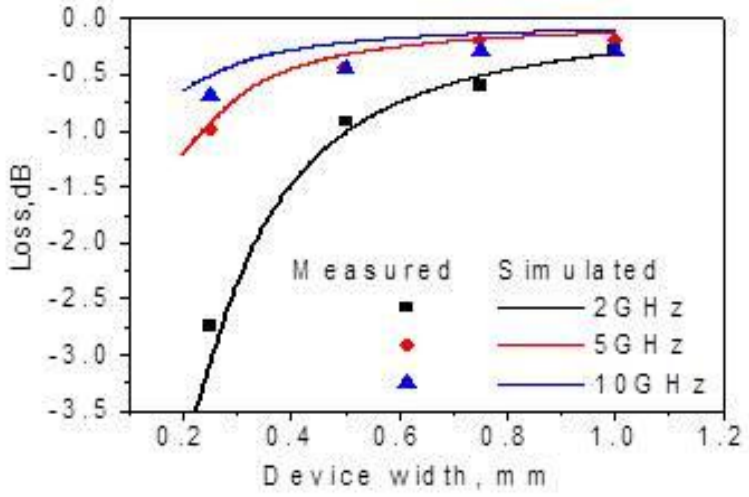

Figure 4.6 Varactor PL power transmission loss variation over width

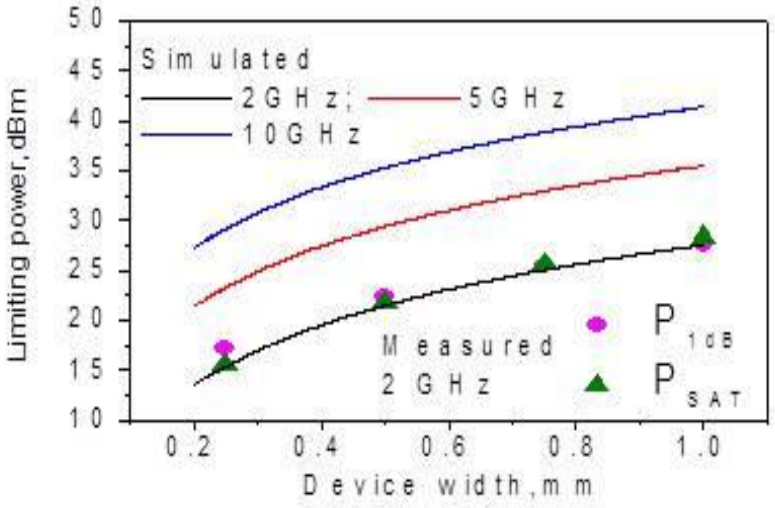

Figure 4.7 Varactor PL limiting power variation over device width

Power dependencies were measured at 2 GHz .The results are shown in Figs. 4.7 and 4.8. The 2 GHz limiting power increases with the device width from 17 dBm for W=0.25mm to 27 dBm for W = 1 mm. At higher frequencies, limiting powers reach 40 dBm. Developed C3 PL shows very small difference between 1 dB compression and saturation powers thus featuring very sharp power limitation. It is believed that the

observed power roll-off beyond the saturation point is due to self-heating. The C3 limiting power can be adjusted using structures with different V_{PO} and/or C3 capacitance. The achieved C3 PL loss of 0.2 – 0.67 dB at 10 GHz is lower compared to other PL types, e.g. 1.5 dB reported for Schottky diode PLs [49].

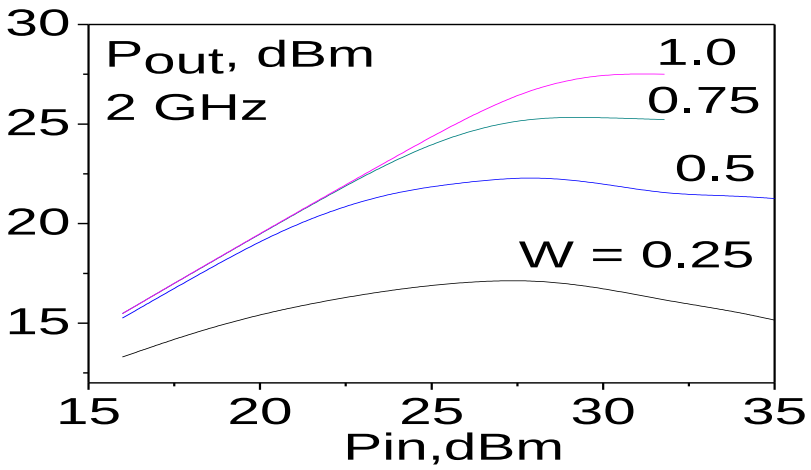

Figure 4.8 C3 PL power transmission

The 100 hours 24 dBm CW stress showed (Fig 4.9) the output power variations within 0.5 dB; these variations only occurred during the first 30 minutes; after that the power remained stable.

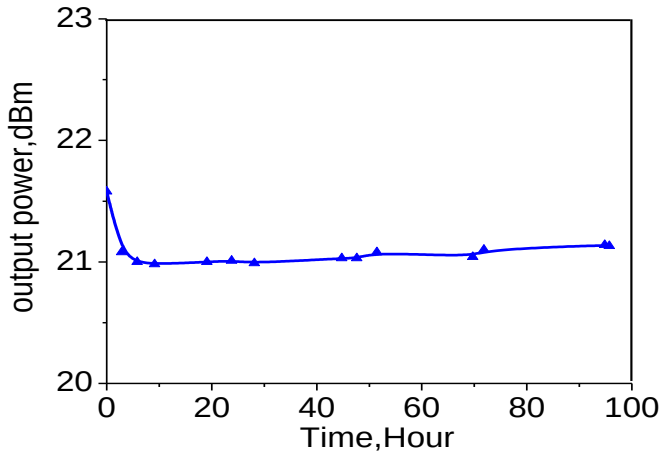

Figure 4.9 Varactor PL power stress stability measurement

The temperature dependence test (limited by the probe station specifications) was performed from 25 ^{o}C to 200^{o}C. The measurement revealed ≈ 0.5 dB loss increase at 200^{o} C compared to room temperature (Fig 4.10).

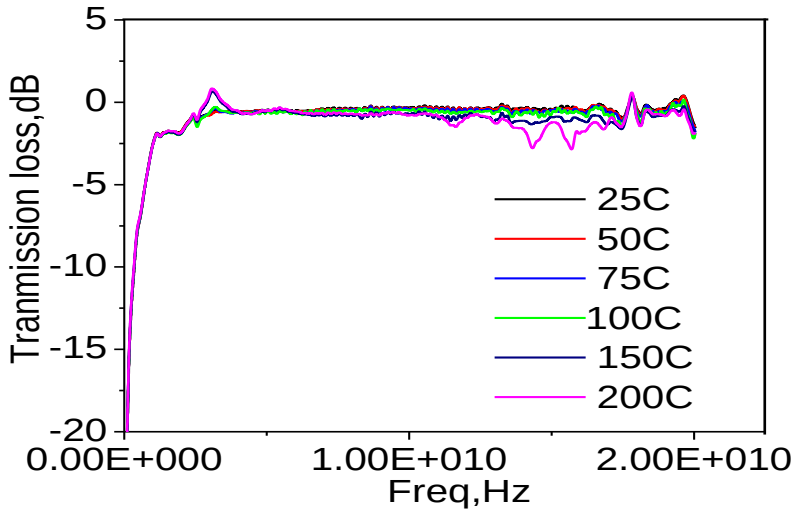

Figure 4.10 Varactor PL temperature stability measurement

An important characteristic of a PL is the maximum sustainable power. This power is limited by the device breakdown. For the fabricated C3 varactors, the breakdown voltage of 95 V was measured. This voltage is equivalent to 49.5 dBm power across the varactor. If required, the maximum power can be further increased using larger C3 electrode separation.

4.4 Conclusions

Low-loss RF PL based on C3 AlGaN/GaN varactor was demonstrated for the first time. C3 varactor is planar, anneal-free, gate alignment-free device; the limiting powers range from 17 to 40 dBm depending on the device width and frequency. The C3 PL shows stable performance under CW stress with output power variations within 0.5 dB during 100 hours stress and operating temperatures up to 200^{o} C.

CHAPTER 5

CONCLUSION AND FUTURE WORK

5.1 Summary of Results

In this dissertation, Low-loss RF control element using two-terminal III-Nitride heterostructure varactor with capacitively-coupled contacts (C3) was demonstrated for the first time. This varactor can be used as a RF switch as well as a power limiter (PL) or other control device type.

This C3 varactor consists of two electrodes deposited on top of an AlGaN/GaN heterostructure forming capacitors between the electrode and the 2DEG channel. C3 electrodes allow for efficient RF signal injection into the 2DEG channel with low equivalent impedance at high frequencies. The C3 varactor has simple planar structure fully compatible with MMICs. The GaN C3 varactors have significant advantages over GaN heterostructure field-effect transistors (HFETs) as they allow for shorter channel, do not have gates or ohmic contacts and hence the fabrication is alignment- and anneal - free, they do not consume DC current and provide the DC block.

The varactor operation as RF Switch and RF power limiter were described in detail. Device design and optimization procedures carried out for high performance C3 varactor based RF switch and power limiter are also shown in detail.

The fabricated SPST C3 switch exhibits 0.8 dB insertion loss and 27 dB isolation at 18 GHz. The maximum switching power extrapolated at 18 GHz is around 38 dBm.

The obtained C3 switch loss compares favorably with the reported 18 - 20 GHz results, e.g. 1.5 dB for GaN HFET or 2 dB for ferrite varactor switch. The switching speed was found to be in the range of 500-800 ns which is very fast compared to other device types such as 200-3000 us for thermal/magnetic MEMS switches.

The fabricated varactor PLs show 0.2-0.7 dB loss, which is lower compared to other PL types, e.g. 1.5 dB reported for Schottky diode PLs and limiting powers in the range from 17 to 40 dBm depending on the device width and frequency with breakdown voltage of 95 V for the device with the 2 um spacing.

The C3 switch and PL show superior performance compared to other known types. The fabricated C3 PLs and switches showed the output power variations within 0.5 dB during 100 hours 24 dBm CW stress. They also demonstrated as low as 0.5 dB loss degradation at 200^{o} C as compared to the room temperature performance.

The achieved results show that novel C3 RF components have superior performance characteristics, can operate in a broad frequency range, and have a great potential for high-performance MMICs.

5.2 Future Work

Firstly, as the C3 varactor SPST RF switch showed promising results, to further explore the varactor performance other popular configurations of practical switches such as SPDT switch can be designed. Fig 5.1 and 5.2 show the SPDT layout and some initial simulation results for C3 varactor SPDT RF switch. For the SPDT, the total width of the series and shunt varactors comprising the switch, W_{SER}= 0.25mm and W_{SHT} = 0.20 mm.

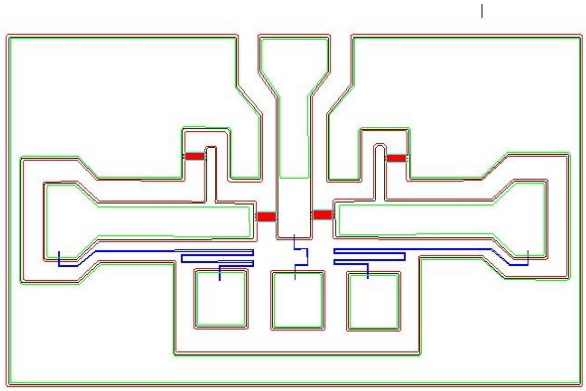

Figure 5.1 C3 Varactor SPDT switch layout

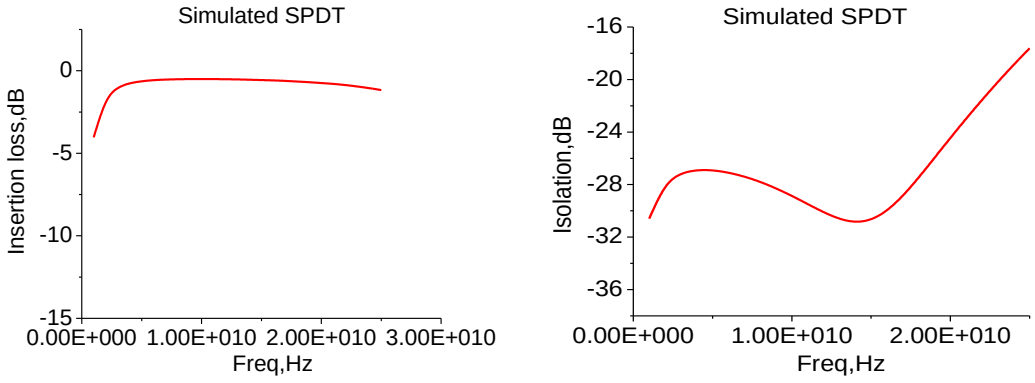

Figure 5.2 Simulated IL and IS plots for C3 varactor SPDT switch

Further analysis, simulations and experiments are needed to be carried out in order to find the optimized layout for such design, considering insertion loss, isolation and power performance.

Secondly, the device performance can be analyzed for other substrate materials, such as SiC, Si etc. In this dissertation all of the developed devices were fabricated on Sapphire substrate. It might be an interesting research to see how the device behavior changes with different substrate materials which might impact the overall device performance. Figure 5.3 shows the power performance of C3 varactor test elements fabricated on SiC and Sapphire substrates.

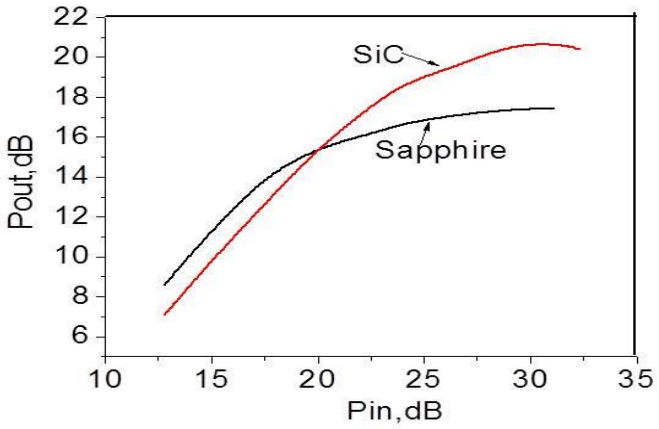

Figure 5.3 Varactor PL power transmission for devices on different substrates

Finally, the non-linearity measurement can be performed to observe how the harmonics generation impacts the overall device performance.

REFERENCES

1.Ishida H, Hirose Y, Murata T, Ikeda Y, Matsuno T, Inoue K, et al, A high RF switch IC using AlGaN/GaN HFET with single-stage configuration. IEEE Transaction on Electron Devices, Vol 52, No. 8, pp. 1893-1899, August 2005.

2. S. Farzaneh and AR Sebak, Microwave Sampling Beam former Prototype Verification and Switch Design, IEEE Transactions on Microwave Theory and Techniques 57 (2009), no. 1, pp.36-44.

3. P.W. Wong and I.C. Hunter, Parallel-Coupled Switched Delay Line (SDL) Reconfigurable Microwave Filter, IEEE MTT-S Int. Microwave Symp. Dig, 2009, pp. 513-516.

4. Robert H. Caverly and Gerald Hiller, Distortion in p-i-n Diode Control Switches, IEEE Transactions on Microwave Theory and Techniques, Vol. 35, No. 5, pp. 492-501, May 1987.

5. Alan J. Fenn, Donal H. Temme, William P. Delaney and William E. Courtney, The Development of Phased–Array Radar Technology, Lincoln Laboratory Journal, Vol.12, No.2, pp. 321-340, 2000.

6. N. Camara, K. Zekentes, LP Romanov, AV Kirillov, MS Boltovets, KV Vassilevski and G. Haddad, Microwave pin diodes and switches based on 4H-SiC, IEEE Electron Device Letters 27 (2006), no. 2, pp.108-110.

7. EW Jacobs, DW Fogliatti, H. Nguyen, DJ Albares, CT Chang, and CK Sun, Photo-injection pin diode switch for high-power RF switching, IEEE Transactions on Microwave Theory and Techniques 50 (2002), no. 2, pp.413-419.

8. J. Park, ES Shim, W. Choi, Y. Kim, Y. Kwon, and D.I. Cho, A Non-Contact-Type RF MEMS Switch for 24-GHz Radar Applications, Microelectromechanical Systems, Journal of 18 (2009), no. 1, pp.163-173.

9. C.H. Kim, Y. Hong, S.H. Lee, S. Kwon, and I.S. Song, Force Coupled Electrostatic RF MEMS SP3T Switch, IEEE MTT-S International Microwave Symposium Digest, 2006, pp. 1281-1284.

10. K. Miyatsuji, S. Nagata, N. Yoshikawa, K. Miyanaga, Y. Ohishi, and D. Ueda, AlGaAs high-power RF single-pole double-throw switch IC for digital mobile communication system, 1994 IEEE International Solid-State Circuits Conference, 1994.Digest of Technical Papers, 41st ISSCC, 1994, pp. 34-35.

11. T. Yamashita, K. Fukamachi, and S. Kemmochi, Low distortion and compact RF switch circuitry with the combination of PIN-diode and GaAs-FET for GSM quartet-band cellular phone, 34th European Microwave Conference, vol. 2, 2004.

12. D. Smith, D. Heston, and D. Allen, Designing high-power limiter circuits with GaAs PIN diodes, IEEE MTT-S Digest, pp.329-332, 1999.

13. NV Drozdovski and RH Caverly, GaN-based high electron-mobility transistors for microwave and RF control applications, IEEE Transactions on Microwave Theory and Techniques 50 (2002), no. 1 Part 1, 4-8.

14. H. Ishida, Y. Hirose, T. Murata, Y. Ikeda, T. Matsuno, K. Inoue, Y. Uemoto, T. Tanaka, T. Egawa, and D. Ueda, A high-power RF switch IC using Al- GaN/GaN HFETs with single-stage configuration, IEEE Transactions on Electron Devices 52 (2005), no. 8, 1893-1899.

15. A. Koudymov, S. Rai, V. Adivarahan, M. Gaevski, J. Yang, G. Simin, and MA Khan, Monolithically integrated high-power broad-band RF switch based on III-N insulated gate transistors, IEEE Microwave and Wireless Components Letters 14 (2004), no. 12, 560-562.

16. O. Ambacher, J. Smart, J. R. Shealy, N. G. Weimann, K. Chu, M. Murphy, R. Dmimitrov, L. Wittmer, M. Stutzmann, W. Rieger and J. Hilsenbeck, Two-dimensional electron gases induced by spontaneous and piezoelectric polarization charges in N-and Ga face AlGaN/GaN Heterostructures, Journal of Applied Physics, Vol. 85, No. 6, pp. 3222-3233, March 1999.

17. M. A. Khan, A. Bhattarai, J. N. Kuznia, and D. T. Olson, High electron mobility transistor based on a GaN-AlxGa1-xN heterojunction, Appl. Phys. Lett. Vol. 63, No. 9, pp.1214-1215, August 1993.

18.U. Mishra, GaN-Based RF Power Devices and Amplifiers, Proc. IEEE Vol. 96, No. 2, pp.287-305, February 2008.

19. A. Koudymov, X. Hu, K. Simin, G. Simin, M. Ali, J. Yang and M. A. Khan, Low Loss High Power RF Switching Using Multifinger AlGaN/GaN MOSHFETs, IEEE Electron Device Letters, Vol. 23, No. 8, pp. 449-451, August 2002.

20. R. Gaska, J. Yang, D. Billingsley, A. Sattu, X.Hu, J. Deng, M. Shur, B. Khan, G. Simin,H. Y. Wong, N. Braga and R. Mickevicius, Insulated-Gate Integrated III-Nitride RF Switches, 2011 IEEE Compound Semiconductor IC Symposium, October 2011.

21. M. Kuroda, T. Ueda and T. Tanaka, Nonpolar AlGaN/gAm Metal Insulator Semiconductor Hetreojunction Field Effect Transistor with normally OFF operation, IEEE Transaction on Electron Devices, Vol. 57, No. 2, pp. 368-372, February 2010.

22. G. Simin, B. Khan, J. Wang, A. Koudymov, M. Gaevski, R. Jain, J. Yang, X. Hu, R. Gaska and M. Shur, Multigae GaN RF Switches With Capacitively Coupled Contacts, IEEE Electron Device Letters, Vol. 30, No. 9, pp. 895-897, September 2009.

23. A. K. Sattu, J. Yang, R. Gaska, M. B. Khan, M. Shur and G. Simin, Small and Large Signal Performance of III-Nitride RF Switches With Hybrid Fast/Slow Gate Design, IEEE Microwave and Wireless Components Letters, Vol. 21, No. 6, pp. 305-308, June 2011.

24. SJ Cai, R. Li, YL Chen, L. Wong, WG Wu, SG Thomas, and KL Wang, High Performance AlGaN/GaN HEMT with improved Ohmic contacts, Electronics Letters 34 (1998), 2354.

25. L. Wang, F.M. Mohammed, and I. Adesida, Dislocation-induced nonuniform interfacial reactions of Ti/ Al/ Mo/ Au ohmic contacts on AlGaN/ GaN heterostructure, Applied Physics Letters 87 (2005), 141915.

26. MW Fay, G. Moldovan, PD Brown, I. Harrison, JC Birbeck, BT Hughes, MJ Uren, and T. Martin, Structural and electrical characterization of AuTiAlTi/AlGaN/GaN ohmic contacts, Journal of Applied Physics (2002), 92-94.

27. D. Qiao, LS Yu, L. Jia, PM Asbeck, SS Lau, and TE Haynes, Transport properties of the advancing interface ohmic contact to AlGaN/GaN heterostructures, Applied Physics Letters 80 (2002), 992.

28. L. Wang, D.H. Kim, and I. Adesida, Direct contact mechanism of Ohmic Metallization to AlGaN/GaN heterostructures via Ohmic area recess etching, Applied Physics Letters 95 (2009), 172107.

29. Y.L. Lan, H.C. Lin, H.H. Liu, G.Y. Lee, F. Ren, S.J. Pearton, M.N. Chang, and J.I. Chyi, Low-resistance smooth-surface Ti/Al/Cr/Mo/Au n-type Ohmic contact to AlGaN/GaN heterostructures, Applied Physics Letters 94 (2009), 243502.

30. G. Simin, A. Koudymov, Z.J. Yang, V. Adivarahan, J. Yang, and MA Khan, High power RF switching using III-nitride metal-oxide-semiconductor heterojunction capacitors, IEEE Electron Device Letters 26 (2005), no. 2, 56-58.

31. G. Simin, Z.J. Yang, A. Koudymov, V. Adivarahan, J. Yang, and M.A. Khan, III-nitride transistors with capacitively coupled contacts, Applied Physics Letters 89 (2006), 033510.

32. A. Koudymov, N. Pala, V. Tokranov, S. Oktyabrsky, M. Gaevski, R. Jain, J. Yang, X. Hu, M. Shur, R. Gaska, et al., HfO2 III-Nitride RF Switch With Capacitively Coupled Contacts, IEEE electron device letters 30 (2009), no. 5.

33. NQ Zhang, S. Keller, G. Parish, S. Heikman, SP DenBaars, and UK Mishra, High breakdown GaN HEMT with overlapping gate structure, IEEE Electron Device Letters 21 (2000), no. 9, 421-423.

34. M. Marso, M. Horstmann, H. Hardtdegen, P. Kordos, and H. Lüth, Electrical Behaviour of the InP/InGaAs Based MSM-2DEG Diode, Solid-State Electronics Vol 41, pp. 25 - 31 (1997).

35. M. Marso, M. Wolter, P. Javorka, A. Fox and P. Kordos, AlGaN/GaN varactor diode for integration in HEMT circuits, El. Lett. V. 37, 1476-1479 (2001).

37. G. Simin, V. Adivarahan, A. Koudymov, Z-J. Yang, S. Rai, J. Yang and M. Asif Khan, High-Power RF Switching using III-Nitride Metal-Oxide-Semiconductor Heterojunction Capacitors, IEEE El. Dev. Lett. V.26, N2, 56-58 (2005).

38. G. Simin, M. Shur and R. Gaska, Semiconductor Device and Circuit Having Multiple Voltage Controlled Capacitors, US Patent US7547939 B2, publ. June 16, (2009).

39. Transmission Lines and Wave Propagation, by P. Magnusson, A. Weisshaar, V. Tripathi and G. Alexander, Ch.4, ISBN: 0849302692, CRC Press, 2001.

40. Z. Yang, J. Wang, X. Hu, J. Yang, G. Simin, M. Shur, and R. Gaska, Current Crowding in High Performance Low-Loss HFET RF switches, IEEE El. Dev. Lett. V. 29, 15-17 (2008).

41. Q. Fareed, R. Gaska and M. S. Shur, Methods of Growing Nitride-Based Film Using Varying Pulses, patent US7192849, March 20 (2007).

42. C. Cambell et al, "Wideband High Power GaN on SiC SPDT Switch MMICs", IMS 2010, pp-145-148, 2010.

43. G. Subramanyam, F. Ahamed, and R. Biggers, A Si MMIC Compatible Ferroelectric Varactor Shunt Switch for Microwave Applications, IEEE Microwave & Wireless Components Lett., V. 15, 739-741 (2005).

44. P.D Grant, R.R. Mansour, and M.W Denfoff, A Comparison between RF MEMS Switches and Semiconductor Switches.

ftp://78.38.77.30/cee/baganji/RF%20switch/mems-switch-2002.pdf.

45. **F. Jahan**, Y-H. Yang, M. Gaevski, J. Deng, R. Gaska, M. Shur, and G. Simin, 2 – 20 GHz Switch using III-Nitride Capacitively-Coupled Contact Varactors, IEEE El. Dev. Lett, Vol.34 No.2, pp.208-210.

46. **F. Jahan**, Y-H. Yang, M. Gaevski, J. Deng, R. Gaska, M. Shur, and G. Simin, High Performance RF Components Using Capacitively-Coupled Contacts Over III-N Heterostructures, Proceedings of 63rd IEEE Electronic Components and Technology Conference, May 2013,pp.2002-2005.

47. **F. Jahan**, M. Gaevski, J. Deng, R. Gaska, M. Shur and G. Simin, RF Power Limiter using Capacitively -Coupled Contacts III-Nitride Varactor, Electronics Letters, Vol. 48 No. 23, pp. 1480-1481.

48. G. Simin, **F. Jahan**, J. Yang, M. Gaevski, X. Hu, J. Deng, R. Gaska and M. Shur, III Nitride microwave control devices and ICs, Semicond. Sci. Technol.28(2013) 074008(8pp).

49. S. Bera, K. Basak, V. Jain, R. Singh, and V. Garg, Schottky Diode-Based Microwave Limiter With Adjustable Threshold Power Level, Microwave and Optical Tech. Lett. V. 52, 2010, pp. 1671 -1673.